



Cancer Cell Resistance to IFN γ Can Occur via Enhanced Double-Strand Break Repair Pathway Activity

Tong Han¹, Xujun Wang², Sailing Shi¹, Wubing Zhang¹, Jue Wang³, Qiu Wu⁴, Ziyi Li¹, Jingxin Fu¹, Rongbin Zheng¹, Jiamin Zhang¹, Qin Tang³, Peng Zhang³, and Chenfei Wang¹

ABSTRACT

The pleiotropic cytokine interferon-gamma (IFN γ) is associated with cytostatic, antiproliferation, and proapoptotic functions in cancer cells. However, resistance to IFN γ occurs in many cancer cells, and the underlying mechanism is not fully understood. To investigate potential IFN γ -resistance mechanisms, we performed IFN γ -sensitivity screens in more than 40 cancer cell lines and characterized the sensitive and resistant cell lines. By applying CRISPR screening and transcriptomic profiling in both IFN γ -sensitive and IFN γ -resistant cells, we discovered that activation of double-strand break (DSB) repair genes could result in IFN γ resistance in cancer cells. Suppression of single-strand

break (SSB) repair genes increased the dependency on DSB repair genes after IFN γ treatment. Furthermore, inhibition of the DSB repair pathway exhibited a synergistic effect with IFN γ treatment both *in vitro* and *in vivo*. The relationship between the activation of DSB repair genes and IFN γ resistance was further confirmed in clinical tumor profiles from The Cancer Genome Atlas (TCGA) and immune checkpoint blockade (ICB) cohorts. Our study provides comprehensive resources and evidence to elucidate a mechanism of IFN γ resistance in cancer and has the potential to inform combination therapies to overcome immunotherapy resistance.

Introduction

Antitumor immunity involves concerted interactions between cytokines and effector cells (1). Interferon-gamma (IFN γ), predominantly secreted by T cells and natural killer (NK) cells, is a crucial effector with pleiotropic effects in antitumor immune responses. Studies have shown the effects of IFN γ on various cancer types (2, 3). IFN γ treatment combined with chemotherapy has been shown to enhance the therapeutic response in patients with ovarian cancer and advanced hepatocellular carcinoma. In addition, IFN γ also plays an important role in immune checkpoint blockade (ICB) therapy (4). ICB therapy with antibodies targeting CTLA-4 or PD-1 could increase IFN γ production in the tumor microenvironment (TME), eliminating cancer cells (5, 6).

The mechanisms of tumor killing by IFN γ have been extensively studied, with JAK/STAT signaling the primary pathway involved (7). Upon binding of IFN γ to its receptors IFNGR1 and IFNGR2, Janus

kinases JAK1 and JAK2 are recruited and activated, which in turn activates the transcription factor STAT1. Phosphorylated STAT1 translocates to the nucleus to modulate the transcription of IFN γ -regulated genes such as *IRF1*. IRF1 functions as a transcription activator of interferon-stimulated response elements (ISRE), leading to the transcription of a large number of secondary response genes. A subset of the target genes are involved in cell-cycle regulation, such as the cyclin-dependent kinase inhibitors p21 and p27, allowing IFN γ to exert direct cytostatic or cytotoxic effects on cancer cells (8). The IFN γ /STAT1 signaling pathway has also been implicated in promoting apoptosis in cancer cells by upregulating the expression of caspase-1, -3, and -8 and enhancing the expression of FAS and FAS ligands (9, 10). In addition, IFN γ signaling in cancer cells can upregulate major histocompatibility complex (MHC) class I expression, thus increasing tumor sensitivity to CD8 $^{+}$ T cell-mediated lysis (11). Furthermore, IFN γ also orchestrates the recruitment of NK cells, T cells, and invariant NK T cells to the TME by triggering the production of the chemokines CXCL9, CXCL10, and CXCL11 (12). Last but not least, IFN γ has been reported to be involved in the inhibition of angiogenesis, impairing the proliferation and survival of endothelial cells, and inducing ischemia in the tumor stroma (13).

Despite the antitumor effect of IFN γ , resistance of cancer cells to IFN γ has also been reported in many studies (14, 15). For example, loss of IFN γ signaling pathways, such as reduced STAT1 activity, JAK1/2 deficiency, and loss of function of IFNGR1/2 and *IRF1*, may reduce the response to IFN γ treatment in cancer cells (16, 17). Suppressor of cytokine signaling (SOCS) proteins, important negative regulators of IFN γ signaling pathways, can block the activity of JAKs directly. Previous studies showed that constitutive activation of SOCS proteins, such as SOCS1 and SOCS3, limits the actions of IFN γ in human melanoma cells (18). In addition, recent reports have shown that PTPN1/2, a protein tyrosine phosphatase, can inhibit IFN γ signaling by dephosphorylating STAT1 and JAK1 (19, 20). These studies indicate that cancer cells can develop IFN γ -dependent pathways to evade IFN γ -mediated killing. However, mutations of the IFN γ signaling pathway in patients are reported in less than 1% of primary tumor cases (21), indicating alternative mechanisms might be used to evade the antitumor effects of IFN γ .

¹Key Laboratory of Spine and Spinal Cord Injury Repair and Regeneration, Ministry of Education, Department of Orthopedics, Tongji Hospital, Frontier Science Center for Stem Cells, School of Life Science and Technology, Tongji University, China. ²SJTU-Yale Joint Center for Biostatistics and Data Science, Department of Bioinformatics and Biostatistics, School of Life Science and Biotechnology, Shanghai Jiao Tong University, Shanghai, China. ³Department of Thoracic Surgery, Shanghai Pulmonary Hospital, School of Medicine, Tongji University, Shanghai, China. ⁴Clinical and Translational Research Center of Shanghai First Maternity and Infant Hospital, Frontier Science Center for Stem Cells, School of Life Sciences and Technology, Tongji University, Shanghai, China.

T. Han and X. Wang contributed equally to this article.

Corresponding Authors: Chenfei Wang, School of Life Science and Technology, Tongji University, 1239 Siping Road, Shanghai 200092, China. Phone: 8621-6598-1195; Fax: 8621-6598-1195; E-mail: 08chenfeiwang@tongji.edu.cn; and Peng Zhang, 507 Zhengmin Road, Shanghai 200433, China. Phone: 8613-5121-85932; Fax: 8613-5121-85932; E-mail: zhangpeng1121@tongji.edu.cn

Cancer Immunol Res 2023;XX:XX-XX

doi: 10.1158/2326-6066.CIR-22-0056

©2023 American Association for Cancer Research

In this study, we systematically evaluated the sensitivity of cancer cells to IFN γ treatment and analyzed pretreatment transcriptomic data to identify potential pathways regulating resistance to IFN γ . Our findings were validated through high-throughput CRISPR screening and custom transcriptomic profiling in a panel of IFN γ -sensitive and -resistant cancer cell lines. Integrative analysis of public TCGA clinical tumor profiles and ICB cohorts indicates the strong clinical relevance of our findings (Fig. 1A).

Materials and Methods

Cancer cell culture and compounds

Cell lines with medium information are listed in Supplementary Table S1. Cancer cells and HEK293T (RRID:CVCL_0063) were purchased from the Cell Bank of Type Culture Collection of the Chinese Academy of Sciences (Shanghai, China) in 2014 to 2016. All cells for experiments were frozen at passages two to five passages after purchase. All cell lines were expanded and frozen at early aliquots, and each were cultured for less than a total cumulative time of 6 months from the time of acquisition to the time of each experiment. Cell culture was performed in RPMI-1640 medium (Gibco, #11875093) or DMEM (Gibco, #11960044), including 10% fetal bovine serum (FBS, Gibco, #10091148), glutamine (Gibco, #25030081), and 1% penicillin/streptomycin (Gibco, #15070063). Cells were cultured in an incubator at 37°C in a humidified atmosphere containing 5% CO₂. All cell lines were tested for *Mycoplasma* regularly using PCR. Cell lines were authenticated by short tandem repeat analysis.

Recombinant Human IFN-gamma protein (rhIFN γ ; catalog No. 285-IF-100) was purchased from R&D Systems on Biocompare.com.

Stocks of ataxia telangiectasia mutated (ATM) kinase inhibitors (KU-55933, S1092) and DNA-PK inhibitors (NU-7441, S2638) were purchased from Selleck.

IFN γ -sensitivity screens

Cancer cells were seeded into 12-well plates (1.5×10^5 /well) overnight and were exposed to different concentrations of rhIFN γ (0, 1, 3, 5, 7, and 10 ng/mL) for 72 hours. Each condition has two replicates. Control cells were cultured without rhIFN γ . After 72-hour culture, we counted the cell number under each concentration and calculated the cell viability. We defined cell viability under 0 ng/mL rhIFN γ as 100%, and cell viability under other concentrations was calculated as follows:

$$\text{Cell viability} = \frac{\text{The number of cells (1, 3, 5, 7, 10 ng/mL)}}{\text{The number of cells on 0 ng/mL}} \times 100\%.$$

According to the change in survival rates under differential IFN γ concentrations, we classified the cell lines into IFN γ -sensitive cell lines and -resistant cell lines. Finally, cell viability < 80% (10 ng/mL) was quantified as an IFN γ -sensitive cell line, and cell viability > 80% (10 ng/mL) was quantified as an IFN γ -resistant cell line.

RNA extraction and RNA-sequencing data analysis

IFN γ -sensitive cell lines—A549, NCIH1437, MDAMB231, A375, and HCC827—and IFN γ -resistant cell lines—MCF7, HCT116, HUH6, HGC827, COLO205, and SW620—were treated with 10 ng/mL IFN γ for 48 hours. All the cell lines without IFN γ treatment were regarded as controls. RNA of all the IFN γ -treated cells and control cells was extracted using TRIzol reagent (Invitrogen Life Technologies, #15596018). Quality and quantity of RNA were analyzed using NanoDrop, agarose gel electrophoresis, and Agilent

2100 (Thermo Fisher Scientific). RNA-seq libraries were prepared using the Hieff NGS Ultima Dual-mode mRNA Library Prep Kit for Illumina (Yeasen, #12301ES96) and sequenced on Illumina Nova 6000 by Berry Genomics Co. Ltd. Data were aligned to the human reference genome hg38 using STAR (RRID:SCR_004463). RSEM (RRID:SCR_013027) was used to map aligned reads and to generate a gene count matrix. We used DESeq2 (RRID:SCR_015687) to identify the differential expression genes between IFN γ -sensitive cells and IFN γ -resistant cells from the Cancer Cell Line Encyclopedia (CCLE). We regarded the cancer types (e.g., lung cancer and breast cancer) of cell lines as the covariants using the following formula: Design = Cancer type + Cell IFN γ sensitivity. For public data, we downloaded from GEO and used limma to perform differential gene-expression analysis. Gene set enrichment analysis (GSEA) was performed GSEA (RRID:SCR_003199) prereduced mode using stat (DESeq2) or t-value (limma, RRID:SCR_010943) as input and “clusterProfile” R package (RRID:SCR_016884) for visualization (22).

DESeq2 (RRID:SCR_015687) was used to identify the differential expression genes between IFN γ -sensitive cells and IFN γ -resistant cells from the CCLE. The cancer types (e.g., lung cancer and breast cancer) of cell lines were used as the covariants by the following formula: Design = Cancer type + Cell IFN γ sensitivity.

Cloning of sgRNA libraries

For the 6K-cancer library, we used the lentiCRISPR v2 vector (RRID:Addgene_52961) as the backbone. We designed 10 sgRNAs per gene to target ~6,000 genes and added nontargeting sgRNAs as controls. For library construction, we used the same protocol as previous CRISPR screens (23).

Virus and virus infections

Lentiviruses used in this study, including lentiCRISPR v2 vector encoding Cas9 and sgRNAs targeting ~6,000 genes, were packaged in HEK293T cells by cotransfection with psPAX2 (RRID: Addgene_12260) and pMD2.G (RRID:Addgene_12259) as previously described (23). Supernatants were collected at 48 and 72 hours after transfection, passed through a 450-nm filter and added to target cells in the presence of polybrene (8 μ g/mL) (Sigma-Aldrich, #TR-1003-G).

After 48-hour infection, puromycin (2 μ g/mL; Gibco, #A1113803) was used for selection over 2 days, which removed the uninfected cells.

Pooled CRISPR screens and analysis

For the pooled CRISPR screen, IFN γ -sensitive and -resistant cells were used (Supplementary Fig. S1A). A total of 1.2×10^8 cells were infected with the pooled lentiviral library at a multiplicity of infection of 0.3. After puromycin selection, the cells were divided into three groups (day 0, vehicle control, and IFN γ treatment). The cell pellet of the day 0 group was stored at -80°C . For the other two groups, the cells were cultured for 14 days, with/without 10 ng/mL IFN γ individually. The cells were cultured for 14 days, split every 2 to 3 days until the appearance of visibly viable colonies. Genomic DNA was harvested from the live cells using the QIAGEN DNeasy Blood and Tissue Kit (QIAGEN, #69504) according to the manufacturer's instructions. Library construction for NGS was performed by PCR as previously described (24). The PCR products were purified for sequencing on HiSeq X (Illumina). The CRISPR/Cas9 screening data were performed by MAGeCK and MAGeCK-VISPR algorithms. MAGeCK-VISPR calculates the β -score for each gene. The mapping ratio, the number

of missing sgRNAs, and the evenness of sgRNAs were provided (Supplementary Table S2).

Normalization of the screen data sets and definition of essential genes for cell viability

CRISPR screen data sets were normalized using the quantile normalization method, which could make the data comparable across different cell types with different conditions. A gene can be defined as essential when the loss of its function compromises the viability of cells or results in a profound loss of fitness. In our screens, essential genes were highly negatively selected across all the cell lines under vehicle conditions and were strongly enriched in fundamental cellular processes. We regarded the genes whose β -scores were significantly larger than -0.5 under vehicle control as nonessential genes. In our study, a one-sample t test (with $\mu = -0.5$) was used to identify the distribution of gene essentiality. A t -statistic value = 2.5 was used to distinguish essential genes and nonessential genes (Supplementary Fig. S1B). Pathway enrichment of these essential genes was visualized by R package clusterProfiler.

Identification of pathways underlying IFN γ sensitivity or resistance in CRISPR screen

For each cell line, the gene's differential β -score ($\Delta\beta$ -score) between IFN γ treatment versus vehicle control was calculated. The average $\Delta\beta$ -scores were calculated across all selected cell lines. The KO of essential genes would result in a profound survival disadvantage under the vehicle conditions/IFN γ treatment conditions. To minimize the effect of the essential genes on pathway identification, we removed these genes in downstream GSEA. GSEA was utilized to analyze the pathway enrichment based on genes' average $\Delta\beta$ -scores excluding these essential genes (Supplementary Table S3).

Integration of the transcriptomic and CRISPR screen data sets

For transcriptomic data sets, highly expressed pathways of sensitive ($n = 21$) or resistant cell lines ($n = 22$) were identified using their publicly available transcriptomic profiles from CCLE using GSEA. For CRISPR screens, pathway enrichment was identified to assess IFN γ response according to the $\Delta\beta$ -scores using GSEA across all the cancer cell lines. Normalized enrichment scores (NES) were used to quantify the enrichment. Pathways with RNA-seq NESs > 0 (or RNA-seq NESs < 0) indicate genes in such pathways are highly expressed in IFN γ -resistant cell lines (or in IFN γ -sensitive cell lines). In contrast, pathways with Screen NESs > 0 (or Screen NESs < 0) indicate the genes in such pathways have stronger positive selections ($\Delta\beta$ -scores > 0) or stronger negative selections ($\Delta\beta$ -scores < 0) under IFN γ treatment conditions. Thus, we defined "sensitive-related pathways" as those highly expressed in IFN γ -sensitive cancer cell lines, and their deletion in the CRISPR screen obstructed IFN γ killing ($\Delta\beta$ -scores > 0). We also identified "resistant-related pathways," which are highly expressed in IFN γ -resistant cell lines, and inhibition of their genes in the CRISPR screen enhances the IFN γ -mediated killing.

Generation of CRISPR/Cas9 knockout cell lines

To knockout double-strand break (DSB) repair-related genes, CRISPR sgRNA sequences targeting *PAXIP1*, *TP53BP1*, *XRCC4*, *RAD50*, *RAD51*, *BRCA1*, *BRCA2*, or nontargeting control (*AAVS1*) were cloned into a lentiCRISPR v2 vector and confirmed by sequencing. Knockout constructs were cotransfected with pMD2.G and psPAX2 into HEK293FT cells to generate lentivirus. Transfection was performed using X-tremeGENE HP DNA Transfection Reagent (Roche, #6366546001) following the manufacturer's protocol. Lentivirus

was collected at 48 and 72 hours. Then, 786-O cancer cells were infected with a lentivirus, driving the expression of a sgRNA for 48 hours to inactivate each gene individually. After puromycin selection, cells were expanded and collected, and knockout (KO) was verified by western blot analyses. The sequences of individual sgRNA for genes are shown in Supplementary Table S3.

Generation of the overexpressed cell lines

Plasmid lentiCas9-blst was obtained from Addgene (plasmid No. 52962; RRID: Addgene_52962). Different gene sequences (DSB repair genes: *PAXIP1*, *TP53BP1*, and *XRCC4*) were subcloned into a lenti-Cas9-blst vector digested with BamHI (NEB, #R3136V) and XbaI (NEB, #R0145V) via Gibson assembly to generate different gene-expressing vectors (lenti-*PAXIP1*, lenti-*TP53BP1*, and lenti-*XRCC4*). Overexpression of control (lenti-HA tag) was used. Overexpression constructs were cotransfected with pMD2.G and psPAX2 into HEK293FT cells to generate lentivirus. Transfection was performed using X-tremeGENE HP DNA Transfection Reagent (Roche, #6366546001) following the manufacturer's protocol. Lentivirus was collected at 48 and 72 hours. Then, A549 cancer cells were infected with a lentivirus for 48 hours to overexpress each gene individually. After blasticidin S HCl selection (Thermo Fisher Scientific, #A1113903, selection concentration for A549: 5 μ g/mL), cells were expanded and collected, and overexpression was verified by western blot analyses.

Western blotting

For western blotting, cells were lysed in RIPA buffer with protease and phosphatase inhibitor cocktail (Sangon Biotech, #C500005). Protein concentrations were measured with a BCA protein quantity kit (Sangon Biotech, #C503021). Approximately 25 μ g of total protein from each sample was resolved by SDS-PAGE with 4% to 12% 15-well SurePAGE Gel (GenScript, #M00654) and then transferred onto polyvinylidene difluoride membranes (Millipore, #ISEQ00010) following standard procedures. Membranes were blocked with 5% bovine serum albumin (BSA, Sigma-Aldrich, #B2064) in TBST for 2 hours and subsequently incubated with indicated primary antibodies overnight at 4°C according to the manufacturer's recommendations. After three washes with TBST, membranes were incubated with appropriate horseradish peroxidase (HRP)-labeled secondary antibodies for 1 hour at room temperature. The protein bands were detected by using an enhanced chemiluminescence reagent (Smart-ECL Super, #S32500). The images were captured with the Tanon 4600SF chemiluminescent imaging system (Tanon 4600SF). Primary antibodies, PAXIP1 antibody (Abcam; cat. #ab168502, RRID: AB_2893189), TP53BP1 antibody (Cell Signaling Technology; cat. #4937, RRID: AB_10694558), RAD50 antibody (Cell Signaling Technology; cat. #3427, RRID: AB_2176936), RAD51 antibody (Cell Signaling Technology; cat. #8875, RRID: AB_2721109), XRCC4 antibody (Cell Signaling Technology, cat. #23908), BRCA1 antibody (ABclonal; cat. #A11034, RRID: AB_2758380), BRCA2 antibody (Cell Signaling Technology; cat. #10741, RRID: AB_2797730), were used to evaluate protein expression. β -Tubulin antibody (Cell Signaling Technology; cat. #2146, RRID: AB_2210545) was used as a loading control. Goat anti-mouse secondary antibody (Cell Signaling Technology; cat. #7076, RRID: AB_330924) and goat anti-rabbit secondary antibody (Cell Signaling Technology; cat. #7074, RRID: AB_2099233) were used.

Cell proliferation and cell viability assays

786-O cells with *PAXIP1*, *TP53BP1*, *XRCC4*, *RAD50*, *RAD51*, *BRCA1*, and *BRCA2* KO or nontargeting control (*AAVS1*) KO were

seeded in 96-well plates (500 cells per well, $n = 3$) and cultured 24 hours before IFN γ treatment (10 ng/mL). Upon the addition of IFN γ , cell growth was monitored on days 1, 3, 5, and 7. At each time point, the medium was aspirated and fresh culture medium was added to the wells. CCK-8 reagent (10 μ L, DOJINDO, #1310) was added to each well, and the plate was incubated at 37°C with 5% CO₂ for 1 hour. The optical density at 450 nm was measured to monitor cell growth.

A549 overexpressing *PAXIP1*, *TP53BP1*, and *XRCC4* or lenti-HA tag were seeded in 96-well plates (500 cells per well, $n = 6$) and cultured for 24 hours before IFN γ treatment (10 ng/mL). Upon the addition of IFN γ , cell growth was monitored on days 1, 3, 5, and 7. At each time point, the medium was aspirated and fresh culture medium was added to the wells. CCK-8 reagent (10 μ L, DOJINDO, #1310) was added to each well, and the plate was incubated at 37°C with 5% CO₂ for 1 hour. The optical density at 450 nm was measured to monitor cell growth.

The activity levels of single agents and combinations were determined by Cell Counting Kit-8 (CCK-8). 786-O kidney cancer cells and HCT116 colon cancer cells were seeded in 96-well plates (500 cells per well for 786-O and 1,000 cells per well for HCT116), cultured 24 hours before compound addition (KU-55933, 7 μ mol/L and/or 10 ng/mL IFN γ) and biologically replicated three times. Upon the addition of the drug, cells were incubated for 7 days. After 7 days of culture, the medium was aspirated and fresh culture medium was added to the wells. CCK-8 reagent (10 μ L) was added to each well, and the plate was incubated at 37°C with 5% CO₂ for 1 hour. The optical density at 450 nm was measured to monitor cell viability. The cell survival rate was calculated as follows: cell viability rate (%) = [(As – Ab)/((Ac – Ab)] × 100%, in which As = experimental group (culture medium and the compound); Ab = blank well (culture medium); AC = control well (culture medium and 1% DMSO).

Cell colony formation

786-O with *PAXIP1*, *TP53BP1*, *XRCC4*, *RAD50*, *RAD51*, *BRCA1*, and *BRCA2* KO or nontargeting control (AAVS1) KO were seeded in 6-well plates (500 cells per well for 786-O) and attached for 24 hours before IFN γ treatment (10 ng/mL, IFN γ treatment). The cells were maintained for 2 weeks. Colonies of cells were washed with PBS (Gibco, #20012027) and then fixed with 1% methanol (Sangon Biotech, #A506806). The colonies were stained with 1% crystal violet (Sangon Biotech, #E607309) and imaged using a camera.

A549 overexpressing *PAXIP1*, *TP53BP1*, and *XRCC4* or lenti-HA tag were seeded in 6-well plates (500 cells per well for A549) and attached for 24 hours before IFN γ treatment (10 ng/mL, IFN γ treatment). The cells were maintained for 2 weeks. Colonies of cells were washed with PBS and then fixed with 1% methanol. The colonies were stained with 1% crystal violet and imaged.

786-O and HCT116 were seeded in 6-well plates (500 cells per well for 786-O and 1,000 cells per well for HCT116) and attached for 24 hours. The cells were maintained for 2 weeks after being treated with KU-55933 (ATM inhibitor, 7 μ mol/L) or NU-7441 (DNA-PK inhibitor, 2 μ mol/L/1 μ mol/L) or KU-55933 (ATM inhibitor, 7 μ mol/L) + IFN γ (10 ng/mL) or NU-7441 (DNA-PK inhibitor, 2 μ mol/L/1 μ mol/L) + IFN γ (10 ng/mL). Colonies of cells were washed with PBS (Gibco, #20012027) and then fixed with 1% methanol (Sangon Biotech, #A506806). The colonies were stained with 1% crystal violet (Sangon Biotech, #E607309) and imaged using a camera.

Immunofluorescence imaging

IFN γ -sensitive cells—A549 and A375—and IFN γ -resistant cells—786-O and HCT116—were grown on glass coverslips and were treated with IFN γ (10 ng/mL) or vehicle control for 48 hours. Then, cells were

washed with PBS and fixed in 4% paraformaldehyde in PBS for 30 minutes at room temperature. Cells were permeabilized in 0.2% Triton X-100 for 20 minutes, followed by blocking for 30 minutes with 5% BSA (Sigma-Aldrich, #B2064). Coverslips were then incubated with primary antibody (Phospho-Histone H2A.X antibody, Cell Signaling Technology; cat. #9718, RRID:AB_2118009) overnight at 4°C in a humidified chamber, followed by incubation with a secondary antibody for 1 hour (Thermo Fisher Scientific; cat. #A10523, RRID: AB_2534032). Primary and secondary antibodies were diluted in a blocking buffer, and all incubations were performed at room temperature. Coverslips were mounted using ProLong Diamond Antifade Mountant with DAPI (ThermoFisher, #P36971). All images were captured using a fluorescence microscope (Echo Revolved). The number of γ -H2AX-positive puncta was quantified using ImageJ (RRID:SCR_003070). Three independent experiments with three biological replicates per group were performed.

Drug synergy analysis

The SynergyFinder (RRID:SCR_019318) package was used to assess the drug synergy. The synergy scores were based on the Bliss model (25, 26).

In vivo experiment

HCT116 cells (5×10^6) were resuspended in Hank's Balanced Salt Solution (Gibco, #1417112) and injected subcutaneously into the right flank of 6- to 8-week-old female BALB/c nude mice (RRID: IMSR_APB:4790). Seven to 9 days after subcutaneous injection of tumor cells, when the volume of the tumor was approximately 100 mm³, mice were randomly divided into six treatment groups ($n = 6$ mice per group): ATM inhibitor alone in PBS (20 or 30 mg/kg, six mice/group) or vehicle, IFN γ alone (1×10^7 IU/kg, six mice/group) or vehicle and combination of IFN γ (1×10^7 IU/kg, six mice/group) and ATM inhibitor (20 or 30 mg/kg). ATM inhibitor was dissolved in 5% DMSO + 40% PEG300 + 5% Tween 80 and 50% ddH₂O and was administrated at 20 or 30 mg/kg via intraperitoneal injection every 2 days for 3 weeks. IFN γ (1×10^7 IU/kg) was used for intratumoral injection twice a week for 3 weeks. Tumors were measured every 3 days after grouping. Finally, the tumor volume, tumor weight, and mouse body weight were measured. Measurements were assessed manually by assessing the longest dimension (length) and the longest perpendicular dimension (width). Tumor volume was calculated using the formula $\frac{1}{2} \times \text{length} \times \text{width}^2$. All mouse experiments were carried out at the Shanghai Youmi Biotechnology Co., LTD. All mouse experimental procedures followed the guidelines of the Biological Research Ethics Committee of Tongji University.

Collection of public data sets and data analysis

Public transcriptomic data sets were downloaded from GEO: GSE85898 and GSE154996. Gene-expression data of IFN γ responder ($n = 3$) and IFN γ nonresponder ($n = 3$) before and after IFN γ stimulation were downloaded from GSE85898. Gene-expression data of the human melanoma cell lines before and after IFN γ stimulation were downloaded from GSE154996 in which wild-type melanoma cells ($n = 45$) and *JAK1/JAK2*-defective melanoma cells ($n = 8$) were used. DESeq2 or Limma was used to perform differential gene-expression analysis. GSEA was performed using GSEA preranked mode using stat (DESeq2) or *t*-value (Limma) as input and “clusterProfile” R package for visualization. Enriched pathways are listed in Supplementary Table S4.

CCLE expression data sets (date: 20180929) were downloaded from <https://portals.broadinstitute.org/cCLE/data>. DESeq2 was used

to perform differential gene-expression analysis. GSEA was performed using GSEA preranked mode using stat as input and “clusterProfile” R package for visualization. The mutation and copy-number variation (CNV) information of CCLE was downloaded from <https://xenabrowser.net/datapages/> (cohort: CCLE, data set ID: ccle/CCLE_copynumber_byGene_2013-12-03). Cells were defined as SSB repair (SSBr) deficient or wild-type according to the mutations and deletion of SSBr genes. The cells with truncating mutations (frameshift indels, nonsense, and splice-site mutations) or copy-number deep deletions (value < -1) in the SSBr genes were defined as SSBr-deficient cells. Wild-type cells were cells without truncating mutations or deletions in DSBr and SSBr genes. Expression of DSB repair genes, especially IFN γ -related DSBr genes and non-IFN γ -related DSBr genes, was evaluated in both SSBr-deficient cells and wild-type cells. A two-sided paired Student *t* test was used to compute the *P* value.

TCGA expression data sets (*n* = 36) were downloaded from <http://firebrowse.org/>. Mutation data and CNV data are collected from <https://xenabrowser.net/datapages/> (cohort: GDC Pan-Cancer, data set ID: GDC-PANCAN.gistic.tsv) using the same method to define the SSBr-deficient samples with truncating mutations or deep deletions (value < -2) and wild-type samples and evaluate the expression of DSB repair genes. A one-sample paired *t* test was used to compute the *P* value.

For the ICB cohorts, we downloaded three data sets with a sample size larger than 40 from Tumor Immune Dysfunction and Exclusion (TIDE) (<http://tide.dfci.harvard.edu>; refs. 27–29). Immune cell infiltration was inferred from bulk RNA-seq data using CIBERSORT (RRID: SCR_016955, <https://cibersort.stanford.edu/>, absolute mode). The effect of *IFNG* expression on patients' outcomes is calculated using Cox-PH regression. According to the median value of *IFNG* expression, patients were divided into *IFNG* high/low expressed cohorts. A Kaplan-Meier plot was used to visualize the survival between the groups. Log-rank test was used to compute the *P* value in survival analysis.

Cox-PH regression to calculate the interaction score with *IFNG*

The TIDE model was developed by Jiang and colleagues. In this model, a regression method was utilized to evaluate the immune cells' dysfunction by testing the interaction between each gene and immune signatures with the adjustment for these clinical cofounders. We applied this model to identify gene association with *IFNG*. In statistics, two variables interact if the effect of one variable depends on other variables, and a multiplication term in a multivariate linear model can test the interaction effect between two variables. Thus, we applied the Cox-PH survival regression to test how the expression of *IFNG* interacts with other genes in the tumor to affect survival outcomes.

$$\begin{aligned} \text{Response} &= a \times \text{IFNG} \times \text{gene} + b \times \text{IFNG} + c \times \text{gene} + d \times \text{cofounders} \\ &= (b + a \times \text{gene}) \times \text{IFNG} + c \times \text{gene} + d \times \text{cofounders} \end{aligned}$$

In this model, the *Response* refers to the patient's survival information (the time to death event). The variable *gene* refers to the expression level of the candidate gene. Within the cox model, other confounders were also taken into account, including tumor mutation (mutation), tumor resection position (tissue), *CD8* expression level, tumor purity (if available), age, and tumor stage. The coefficients *a*, *b*, *c*, and *d* were estimated through model fitting. Because we selected the TCGA data sets (TCGA-SARC, TCGA-SKCM, TCGA-BRCA, and TCGA-BLCA) and clinical data sets in which *IFNG* is favorable for survival, the coefficient *b* is always negative. If *a* > 0, a higher *gene* will flatten the slope (*b* + *a* × *gene*) between *IFNG* and *Response*, suggesting a worse survival. If *a* < 0, a

higher *gene* will sharpen the slope between *IFNG* and *Response*, which means a better survival outcome. Thus, the interaction term between *gene* and *IFNG* could be used to evaluate the beneficial association between *IFNG* and overall survival. DSB repair genes used in our study are listed in Supplementary Table S5.

To further investigate the alterations of DSB repair genes that would influence *IFNG*-mediated survival, we focused on the DSB repair genes, including loss-of-function mutations and deep deletions, and conducted the same interaction model for each gene as the model for expression signatures of DSB repair genes: *Response* = *a* × *IFNG* × *alteration* + *b* × *IFNG* + *c* × *alteration* + *d* × *cofounders* where *IFNG* is *IFNG* expression in tumor samples, *alteration* is the alteration status of DNA-repair genes, where 0 represents the wild-type DSB repair gene, whereas 1 represents DSB repair gene with loss-of-function mutation or deep deletion. We also took other confounders into account as the model above, such as tumor mutation (mutation), tumor resection position (tissue), *CD8* expression level, tumor purity (if available), age, and tumor stage. In our analyses, the samples with truncating mutations (frameshift indels, nonsense, and splice-site mutations) and copy-number deep deletions (value < -1) in DSB repair genes were defined as DSB repair-deficient samples. The interaction coefficient *a* is the parameter required to be estimated, of which a negative value represents that the alteration of a DSB repair gene could attenuate the beneficial effect of *IFNG* on survival.

Statistical analysis

Statistical tests used with the number of replicates and independent experiments are listed in the relevant Materials and Methods sections and figure legends. Statistical analyses were performed either with the R software (RRID:SCR_001905, <http://www.R-project.org/>) or Prism 9 (GraphPad Prism (RRID:SCR_002798)). Statistical analyses gathering more than two groups were performed using ANOVA. For two group, statistical analyses were performed using a two-sided paired *t* test (ns > 0.05; *, *P* ≤ 0.05; **, *P* ≤ 0.01; ***, *P* ≤ 0.001; ****, *P* ≤ 0.0001). A one-sided paired Student *t* test was used to evaluate the expression of IFN γ -related DSBr genes in tumors with wild-type SSBr genes or tumors with SSBr genes deficiency in TCGA (ns > 0.05; *, *P* ≤ 0.05; **, *P* ≤ 0.01; ***, *P* ≤ 0.001; ****, *P* ≤ 0.0001). Log-rank test was applied when assessing the association between the *IFNG* level and overall survival for patients with different expressions of IFN γ -related DSBr genes.

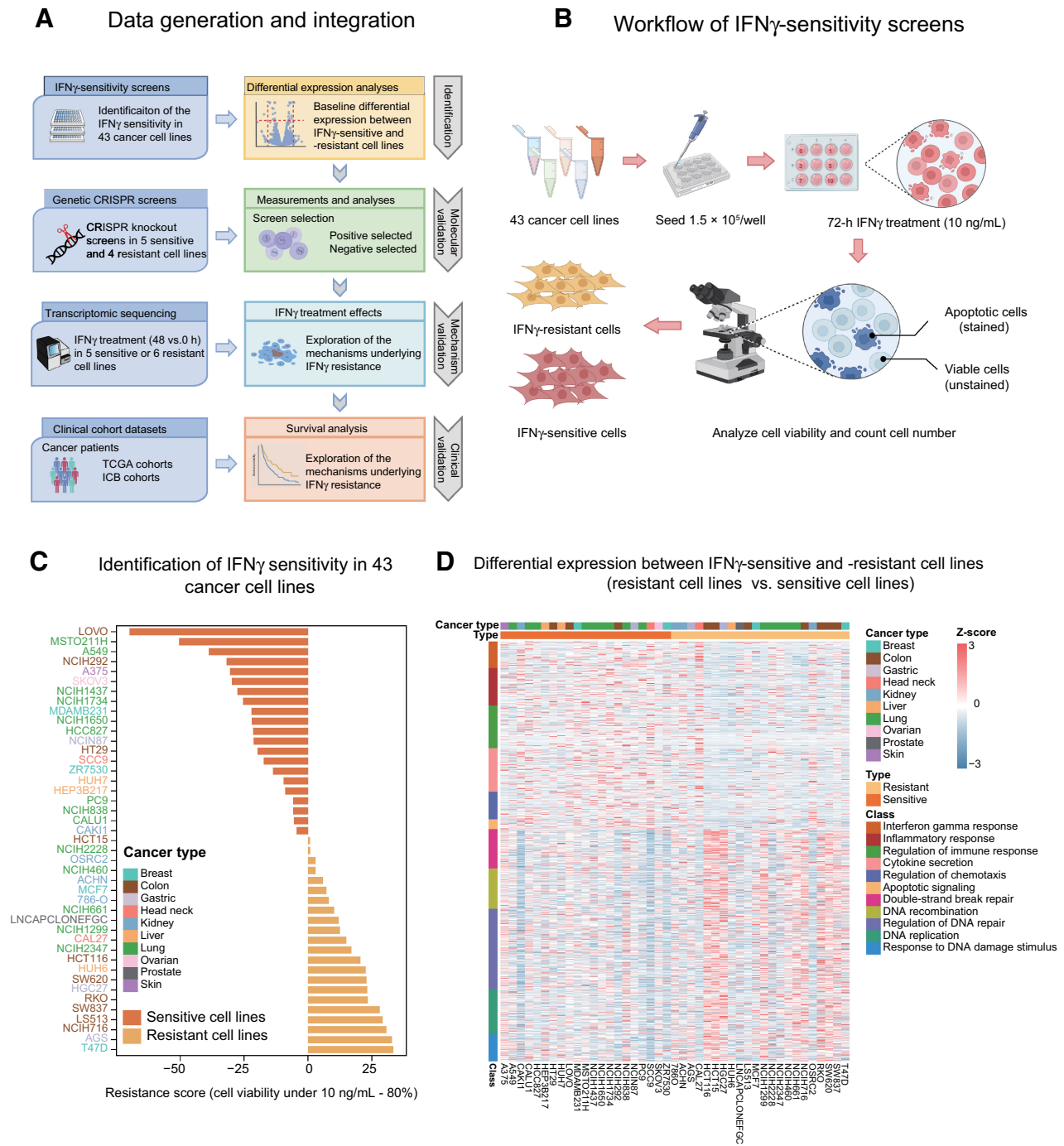
Data availability

All the RNA-seq data and CRISPR screen data sets generated in this study have been deposited to the GEO database under accession number GSE180943. All other data are available in the main text or the supplementary materials or are available from the corresponding author upon reasonable request.

Results

High expression of DSB repair genes in IFN γ -resistant cell lines

To comprehensively understand the molecular mechanisms underlying IFN γ resistance, we conducted IFN γ -sensitivity screens in a total of 43 cancer cell lines, including lung, colon, breast, ovarian, kidney, head neck, prostate, liver, and stomach, which are commonly used models in cancer research (Supplementary Table S1). Cells were treated with increasing concentrations of IFN γ (0, 1, 3, 5, 7, and 10 ng/mL) for 72 hours, and the IFN γ sensitivity of cancer cells was quantified by counting the cell number (Fig. 1B). Cell viabilities under

**Figure 1.**

Transcriptomic characteristics of IFN γ -sensitive and IFN γ -resistant cell lines from CCLE. **A**, Overview of data generation and integration. Identification section: 43 cancer cell lines were used to test the IFN γ sensitivity. Transcriptomic profiles from CCLE were used to identify the transcriptomic characteristics of IFN γ -sensitive cell lines and IFN γ -resistant cell lines. Molecular validation section: functional CRISPR screens were performed in five sensitive cell lines and four resistant cell lines. Mechanism validation section: transcriptomic profiles were generated on five sensitive cell lines and six resistant cell lines before/after IFN γ treatment. Clinical validation section: survival data and clinical data were integrated to validate the biological and clinical significance. **B**, Workflow of IFN γ -sensitivity screens on 43 cancer cell lines. Cancer cells were exposed to different concentrations of IFN γ for 72 hours. Control cells received no treatment. Each condition has two replicates. After 72 hours of culture, counted the cell number under each concentration and calculated the cell viability (details are provided in Materials and Methods). Cell lines with cell viability < 80% (10 ng/mL) were quantified as IFN γ -sensitive cell lines, and cell lines with cell viability > 80% (10 ng/mL) were quantified as IFN γ -resistant cell lines. **C**, IFN γ sensitivity of 43 cancer cell lines, the x-axis represents the IFN γ -resistance score (Resistance score = cell viability under 10 ng/mL – 80%, Resistance score > 0 represents IFN γ -resistant cell lines, Resistance score < 0 represents IFN γ -sensitive cell lines). **D**, Heat map showing the differentially expressed genes (Z-score) between IFN γ -sensitive cell lines ($n = 21$) and IFN γ -resistant cell lines ($n = 22$) using CCLE transcriptomic data sets. DESeq2 was used to call the differentially expressed genes after adjusting the cancer types. Preranked GSEA was used to calculate the enrichment.

differential concentrations were calculated and the cancer cell lines were classified into IFN γ -sensitive ($n = 21$) and IFN γ -resistant ($n = 22$) cell lines accordingly (Fig. 1C; Supplementary Table S1). To address whether differential responses to IFN γ were caused by the inherent molecular characterizations of these cancer cell lines, we examined the transcriptomic difference between the sensitive and resistant cell lines with adjustment for cancer types as covariants using their publicly available transcriptomic profiles from CCLE (Supplementary Table S1). Our analysis revealed that some known regulators of the IFN γ response, such as *IRF1*, *IL18*, *IL1 β* , and *CCR7*, which are involved in IFN γ -mediated signaling pathway and inflammatory response, were highly expressed in IFN γ -sensitive cell lines (Fig. 1D; refs. 30, 31). In addition, we observed that genes such as *RAD50*, *RAD51*, *BRCA1/2*, and *XRCC2-6* were highly expressed in resistant cells (Supplementary Table S1). These genes are involved in DNA-repair pathways, especially DSB repair, suggesting a potential role of DSB repair in mediating IFN γ resistance (Fig. 1D).

CRISPR knockout screens in IFN γ -sensitive and IFN γ -resistant cancer cells

To further assess the molecular mechanisms related to IFN γ resistance, we performed CRISPR KO screens on four IFN γ -resistant cell lines and five IFN γ -sensitive cell lines (Supplementary Fig. S1A). The CRISPR library established in our previous work targeted ~6,000 cancer-related genes (23). After lentiviral library infection and puromycin selection, the cells were treated with IFN γ (10 ng/mL) or vehicle control for 14 days. The sequences encoding the sgRNAs were then PCR-amplified from the transduced cells at day 0 control and after 14 days of culture (IFN γ treatment or vehicle control) and quantified by high-throughput sequencing (Fig. 2A).

CRISPR screen data sets were analyzed using MAGeCK-VISPR (32), an algorithm assessing the sgRNA abundance across different conditions. MAGeCK-VISPR assigns each gene a log fold-change “ β -score” of essentiality in each condition (IFN γ treatment or vehicle control) in comparison with the designated controls (day 0 control; Fig. 2B; Supplementary Table S2). A positive β -score (β -score > 0) of the gene implies a survival advantage upon gene KO (positive selection gene), whereas a negative β -score (β -score < 0) represents a survival disadvantage upon gene KO (negative selection gene). Overall, most genes were consistently positively or negatively selected across all the cell lines under different conditions (Fig. 2C). As expected, negatively selected genes identified as essential for cell survival and proliferation in both conditions were significantly enriched in fundamental biological processes, such as ribosome biogenesis, RNA transcription, and RNA processing (Fig. 2D; Supplementary Fig. S1B and S1C; ref. 33). Meanwhile, positively selected genes were enriched in cell population proliferation, apoptotic process, and regulation of cell death (Supplementary Fig. S1D and S1E; ref. 34). Compared with vehicle control, genes related to IFN γ -mediated immune response and response to cytokine were significantly positively selected under IFN γ treatment conditions, such as *STAT1*, *JAK1/2*, and *IRF1*. These genes are reported to be involved in response to IFN γ and activation of interferon-stimulated genes (ISG; Fig. 2E and F; ref. 35). Altogether, our results reflected the high quality and reproducibility of the CRISPR screen data sets.

CRISPR screens implicated DSB repair-related pathways in driving IFN γ resistance

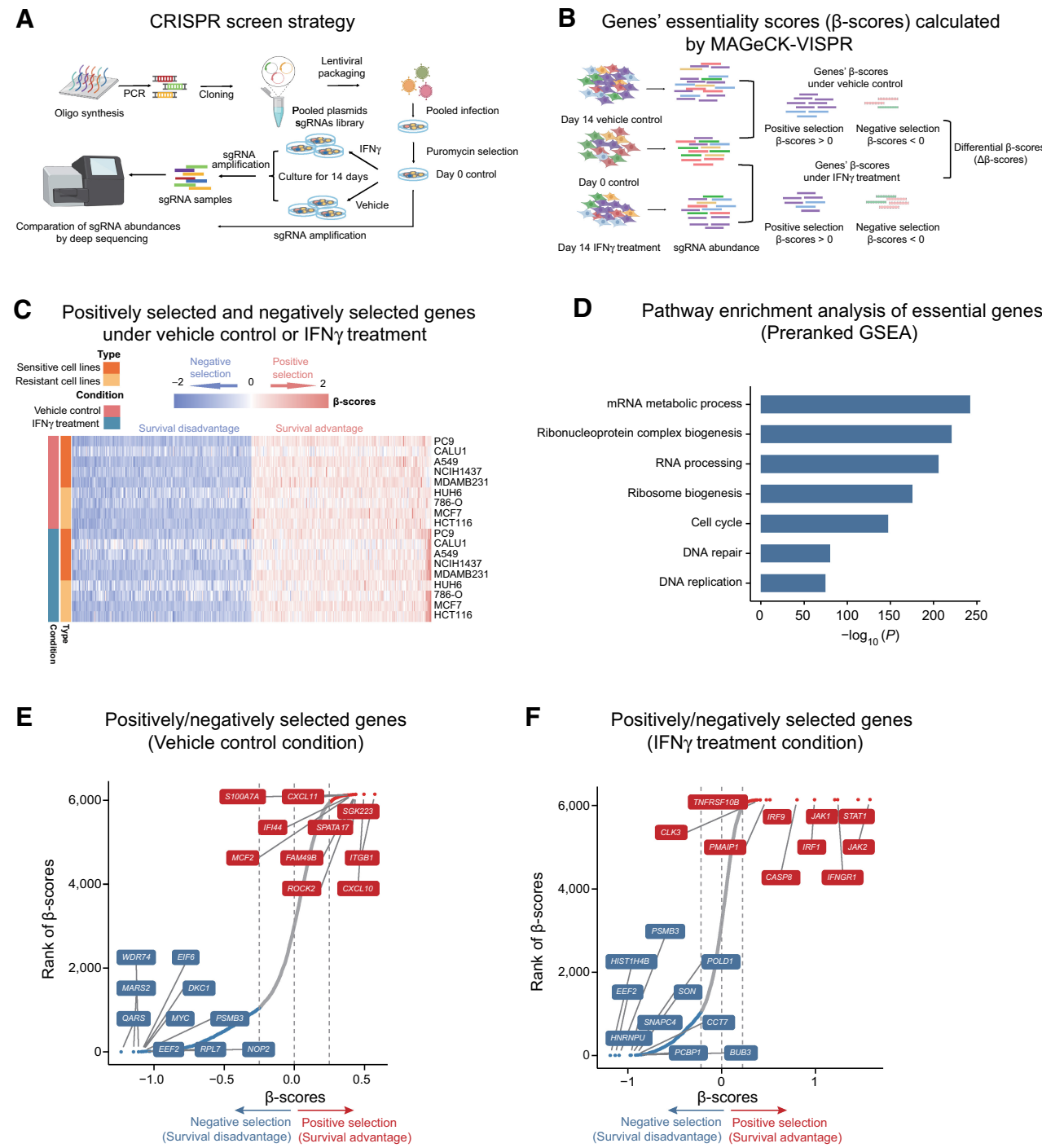
To determine the genes whose loss of function confers IFN γ sensitivity or resistance, we calculated the differential β -score (denoted as $\Delta\beta$ -score) between IFN γ treatment and vehicle control. $\Delta\beta$ -score > 0

(or $\Delta\beta$ -score < 0) reflects a gene whose β -score increased (or decreased) after IFN γ treatment compared with vehicle control, implying cell resistance (or sensitivity) to IFN γ upon gene KO. Our results showed that most genes had consistently positive or negative $\Delta\beta$ -scores across all the cell lines (Fig. 3A) regardless of cell sensitivity (Supplementary Fig. S1F and S1G). For instance, key mediators in the IFN γ cascade, such as *IFNGR1*, *STAT1*, *JAK1/2*, and *IRF1*, exhibited a stronger positive selection ($\Delta\beta$ -score > 0), implying the loss of those genes promoted the cell’s survival advantage to IFN γ treatment (Fig. 3A; Supplementary Fig. S1F and S1G). In contrast, KO of negative regulators of IFN γ signaling, such as *PTPN1/2* (19, 20), *SOCs1* (18), and *TSC1/2* (36), had stronger negative selections ($\Delta\beta$ -score < 0), demonstrating increased cell sensitivity to IFN γ treatment upon gene KO (Fig. 3A). To further understand the pathways involved in IFN γ resistance, we utilized GSEA to analyze pathway enrichment based on genes’ $\Delta\beta$ -scores (Supplementary Table S3). Among the pathways related to stronger negative selection under IFN γ treatment, we found that pathways, including cell-cycle regulation and DNA integrity checkpoint, were highly enriched (Fig. 3B). Besides, genes related to the DSB repair pathway (NES = -1.50, $P = 0.018$) and regulation of DSB repair via homologous recombination (HR; NES = -1.74, $P = 0.004$) also showed significantly decreased β -scores ($\Delta\beta$ -score < 0; Fig. 3C). KO of DSB repair genes increased cell sensitivity to IFN γ treatment ($\Delta\beta$ -score < 0) across all the cell lines, which implied that these DSB repair genes became more essential in the presence of IFN γ treatment (Fig. 3D).

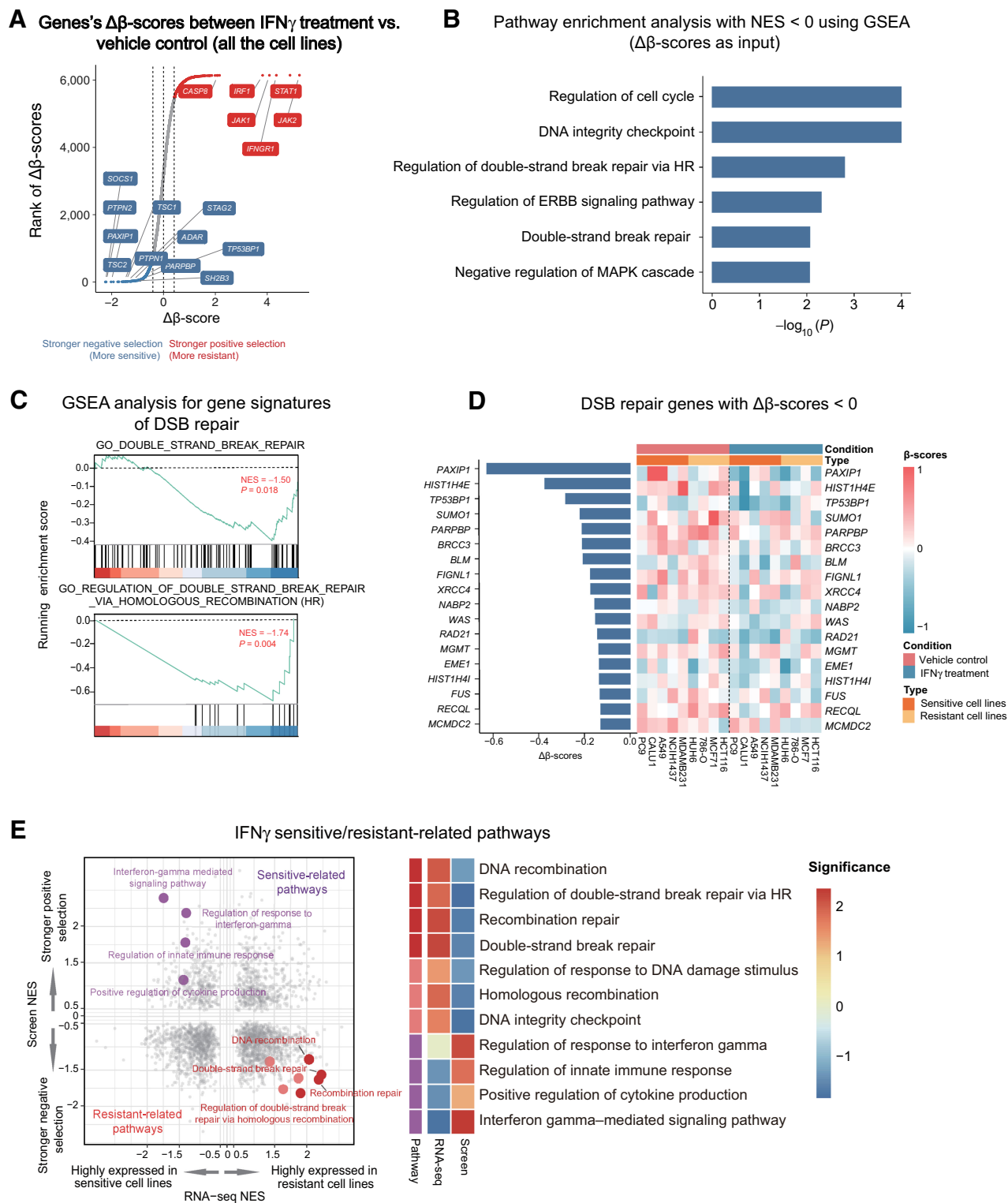
Next, we integrated the transcriptomic and CRISPR screen data sets to better understand the potential pathways driving IFN γ response. We first defined “sensitive-related pathways” as those highly expressed in IFN γ -sensitive cancer cell lines, and their KO obstructed IFN γ -mediated killing ($\Delta\beta$ -scores > 0; Fig. 3E, purple dots in the top left corner). We observed IFN γ -mediated signaling pathways and regulation of innate immune response as “sensitive-related pathways.” We also identified pathways highly expressed in IFN γ -resistant cell lines, and inhibition of their genes enhanced the IFN γ -mediated killing, which we defined as “resistance-related pathways.” The DSB repair pathway was the top resistance-related pathway, which was highly expressed in IFN γ -resistant cancer cell lines, and KO of these genes increased cell sensitivity to IFN γ treatment ($\Delta\beta$ -scores < 0; Fig. 3E, red dots in the bottom right corner). Together, the transcriptomic profiles and CRISPR screen data sets both implicated DSB repair-related pathways in driving IFN γ resistance.

Loss of DSB repair-related genes sensitizes cancer cell lines to IFN γ treatment

To verify that activation of the DSB repair pathway could promote IFN γ resistance, we used independent sgRNAs targeting DSB repair genes in 786-O, which we showed was an IFN γ -resistant cell and exhibited a strong linkage between DSB repair genes and IFN γ resistance (Fig. 1C and Fig. 3D). We introduced multiple sgRNAs targeting DSB repair genes, such as *PAXIP1*, *TP53BP1*, and *XRCC4*, which were the top hits from our screens (Fig. 3D; Supplementary Table S3). Consistent with the screen results, sgRNAs targeting *PAXIP1*, *TP53BP1*, or *XRCC4* depleted the protein level and markedly decreased cell growth and long-term colony formation under IFN γ treatment, suggesting the resistance to IFN γ was attenuated after the loss of DSB repair genes (Fig. 4A–C; Supplementary Fig. S2A and S2B). To further explore whether the high expression of DSB repair genes promotes IFN γ resistance, we overexpressed *PAXIP1*, *TP53BP1*, and *XRCC4* in A549, an IFN γ -sensitive cell line, and observed that overexpression of these genes could increase the resistance to IFN γ .

**Figure 2.**

CRISPR knockout screens in IFN γ -sensitive and IFN γ -resistant cancer cells. **A**, CRISPR screens strategy. **B**, Genes' essentiality scores (β -scores) calculated by MAGeCK-VISPR. MAGeCK-VISPR assesses the sgRNA abundance across different conditions (IFN γ treatment and vehicle control) and assigns each gene a log fold-change "beta-score" of essentiality in each condition in comparison with the designated control (day 0 control). A positive beta-score (β -score > 0) of the gene implies growth advantage after knocking out this gene (positive selection, blue or purple cells), whereas a negative beta-score (β -score < 0) represents a negative selection (green or red cells). Genes' differential beta-scores (denoted as $\Delta\beta$ -scores) between IFN γ treatment versus vehicle control were next calculated. **C**, The heat map shows the positively selected genes (red: survival advantage) and negatively selected genes (blue: survival disadvantage) in IFN γ -sensitive and IFN γ -resistant cells under both conditions. Genes are ranked by the mean value using a one-sample t test across all conditions and cell lines. Top 200 positively (negatively) selected genes to visualize. **D**, Pathway enrichment of essential genes (genes' β -scores < -0.5 under vehicle control, see Materials and Methods for details). Preranked GSEA was used to calculate the enrichment. **E** and **F**, The rank of the genes' β -scores (average β -scores across all the cell lines) under **(E)** vehicle control or **(F)** IFN γ treatment conditions. Red (blue) dots indicate positively (negatively) selected genes.

**Figure 3.**

CRISPR screens implicate DSB repair-related pathways in driving IFN γ resistance. **A**, Genes' $\Delta\beta$ -scores between IFN γ treatment and vehicle control across all the cell lines. Genes with $\Delta\beta$ -scores > 0 (or $\Delta\beta$ -scores < 0) were indicated with red (or blue) dots, respectively. Red (blue) dots indicate a stronger positive (negative) selection under IFN γ treatment that represents the KO of genes was more resistant (sensitive) to IFN γ . **B**, Pathways underlying stronger survival disadvantages using GSEA ($\Delta\beta$ -scores of genes excluding essential genes were calculated across all the cells and $\Delta\beta$ -scores as input). **C**, GSEA for DSB repair pathways with NES < 0 in CRISPR screens ($\Delta\beta$ -scores of genes were calculated across all the cells and $\Delta\beta$ -scores as input). (Continued on the following page.)

treatment (**Fig. 4D**; Supplementary Fig. S2C and S2D). Taken together, our CRISPR screen data suggested that activation of the DSB repair pathway was linked to IFN γ resistance, which was further confirmed by the KO and overexpression validation experiments.

Our analyses demonstrated that enhancement of cell survival might be conferred through the high expression of DSB repair genes. We then investigated differentially expressed genes between IFN γ -resistant and IFN γ -sensitive cell lines before IFN γ treatment. Here, we selected six cancer cell lines from the CRISPR screens (IFN γ -sensitive cell lines: A549, NCIH1437, and MDAMB231; IFN γ -resistant cell lines: MCF7, HCT116, and HUH6). To test whether this mechanism was consistent among different cancer lines, we also selected five additional cell lines from IFN γ -sensitivity screens (IFN γ -sensitive cell lines: A375 and HCC827; IFN γ -resistant cell lines: HGC827, COLO205, and SW620; Supplementary Fig. S2E). In line with the CCLE transcriptomic data sets, some DSB repair genes, such as *RAD50*, *RAD51C*, *BRCA1/2*, and *XRCC2-6*, were also intrinsically highly expressed in IFN γ -resistant cell lines (**Fig. 4E**; Supplementary Fig. S2F). To explore whether KO of these highly expressed DSB repair genes could alter the cellular response to IFN γ treatment, we introduced sgRNAs targeting *RAD50* and *RAD51* and observed that KO of *RAD50* and *RAD51* could also increase the sensitivity of 786-O to IFN γ treatment (**Fig. 4F** and G). KO of *BRCA1* could not overcome the resistance to IFN γ treatment, which was opposite to the phenotypes of KO *BRCA2* (Supplementary Fig. S3A and S3B). This opposite phenotype could be explained by a series of studies that *BRCA1* functions in regulating IFN γ signaling but not *BRCA2* (37, 38). Together, the transcriptomic profiles implicated the activation of DSB repair-related pathways in driving IFN γ resistance, and KO of these DSB repair genes sensitized the cancer cells to IFN γ treatment.

To confirm that DNA damage repair was directly involved in IFN γ resistance, we analyzed expression of the phosphorylated form of H2AX histone (γ -H2AX), an early cellular response to the induction of DSB (Supplementary Fig. S3C–S3E) in both IFN γ -sensitive and IFN γ -resistant cells. At the baseline level, IFN γ -resistant cell lines such as 786-O or HCT116 demonstrated a higher level of γ -H2AX compared with IFN γ -sensitive cell lines such as A549 or A375, implying a higher DNA damage response level in IFN γ -resistant cell lines. γ -H2AX levels were slightly decreased in response to IFN γ treatment in both sensitive and resistant cell lines (Supplementary Fig. S3E). Although DSB repair was slightly suppressed by IFN γ treatment, the γ -H2AX levels of resistance cell lines were still higher than sensitive cell lines and even higher than its baseline level (Supplementary Fig. S3E). Altogether, these results supported an intrinsic high DNA-damage response in IFN γ -resistant cell lines.

Inhibition of DSB repair pathways overcomes resistance to IFN γ *in vitro* and *in vivo*

Given that the transcriptomic data and CRISPR screens revealed the increased dependency of DSB repair genes upon IFN γ treatment, we hypothesized that DSB repair inhibitors might enhance the effects of

IFN γ treatment in resistant cancer cells. KU-55933 is a competitive ATM inhibitor that can attenuate the induction of DNA damage responses. In the presence of a DSB, KU-55933 blocks HR repair signals by decreasing γ -H2AX and *RAD51* foci in human melanoma cells (39). We, therefore, assessed whether there was a synergistic effect between KU-55933 and IFN γ on IFN γ -resistant cells. In the 786-O cell line, ATM inhibitor treatment sensitized IFN γ -resistant cells to IFN γ and enhanced the anticancer effects of the cytokine in both clonogenic assays and cell viability assays (**Fig. 5A** and B). To determine whether such combination treatment is effective in other IFN γ -resistant cells, we also tested the synergy of treatment combination in HCT116 colon cancer cell lines and observed similar effects (**Fig. 5A** and B). The combination treatment of ATM inhibitor with IFN γ was highly synergistic across a broad range of concentrations according to the Bliss independence model in the resistant cell lines (**Fig. 5C**; Supplementary Fig. S4A and S4B).

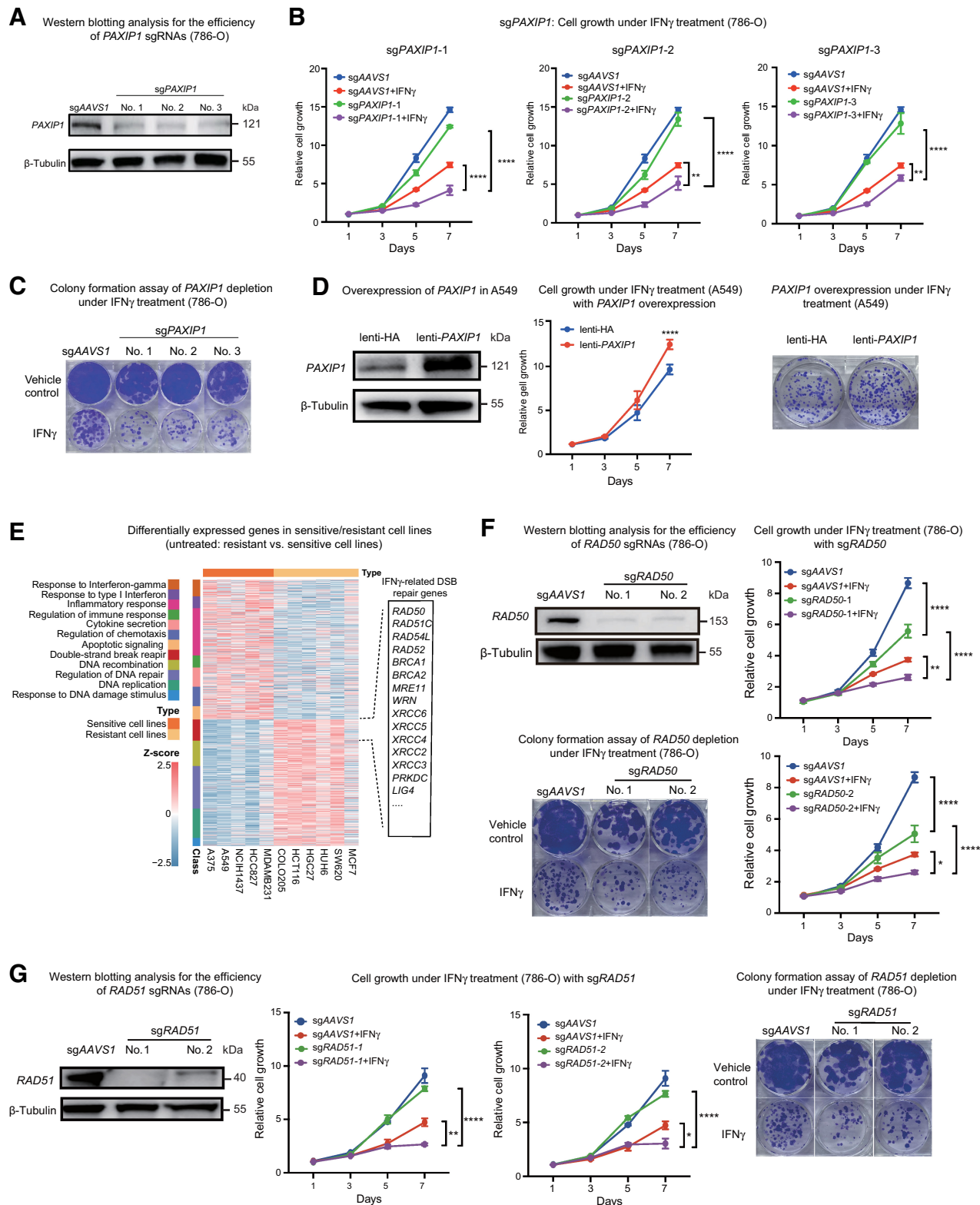
Although ATM plays a more general role in activating the DNA damage response, in mammalian cells, DSBs are predominantly repaired by the nonhomologous end joining (NHEJ) pathway (40). The NHEJ pathway is governed by DNA-dependent protein kinase (DNA-PK) and reconnects the broken DNA ends together directly without using a homologous DNA template. We therefore examined the synergistic effect of DNA-PK inhibitor and IFN γ treatment. In both 786-O and HCT116 cancer cell lines, cotreatment of a DNA-PK inhibitor (NU-7441) and IFN γ significantly decreased cell viability and inhibited cancer cell growth (**Fig. 5D–F**; Supplementary Fig. S4C and S4D).

To evaluate the synergistic effect between DSB repair inhibitors and IFN γ *in vivo*, we generated HCT116 mouse xenografts (**Fig. 5G**). In the HCT116 xenograft mouse model, although the ATM inhibitor and IFN γ as single agents partially suppressed tumor growth, coadministration of the ATM inhibitor (KU-55933) and IFN γ had significantly enhanced antitumor effects, and this combination therapy exhibited a dose-dependent growth inhibition (**Fig. 5H** and I; Supplementary Fig. S4E). In most conditions, mice did not display signs of drug toxicity following the treatment period, and no considerable weight loss was observed between ATM inhibitors versus control groups (Supplementary Fig. S4F). Altogether, these results indicated the combination of DSB repair inhibition and IFN γ treatment as a potential therapeutic strategy to overcome IFN γ resistance *in vivo*.

IFN γ treatment upregulates ISGs in both IFN γ -sensitive and IFN γ -resistant cancer cells

To further explore the potential molecular mechanisms of DSB repair-related pathways in IFN γ resistance, we used the above-mentioned cell lines and evaluated the transcriptome changes upon treatment with IFN γ . We treated the cell lines with 10 ng/mL of IFN γ for 48 hours and examined their transcriptome changes by RNA-seq analysis (Supplementary Fig. S5A; Supplementary Table S4). We observed that immune-related pathways, such as IFN γ -mediated

(Continued.) The corresponding gene set IDs are DOUBLE_STRAND_BREAK_REPAIR (NES = -1.50, P = 0.018) and REGULATION_OF_DOUBLE_STRAND_BREAK_REPAIR_VIA_HOMOLOGOUS_RECOMBINATION (NES = -1.74, P = 0.004). **D**, DSB repair genes with $\Delta\beta$ -scores < 0. Bar plot (left) shows the $\Delta\beta$ -scores, and the heat map (right) shows the β -scores in each cancer cell line under different conditions. **E**, RNA-seq NESs were plotted on the x-axis and RNA-seq NESs > 0 (RNA-seq NESs < 0) indicate genes in such pathways were highly expressed in IFN γ -resistant (IFN γ -sensitive) cell lines. Screen NESs were plotted on the y-axis. Screen NESs > 0 (screen NESs < 0) indicate the genes in such pathways have stronger positive ($\Delta\beta$ -scores > 0) or negative selections ($\Delta\beta$ -scores < 0) under IFN γ treatment conditions. Purple dots (top left corner) represent IFN γ sensitive-related pathways with RNA-seq NESs < 0 and screen NESs > 0. Red dots (lower right corner) represent IFN γ resistant-related pathways with RNA-seq NESs > 0 and screen NESs < 0. The legend of the heatmap is the significance of the “sensitive-related pathway” and “resistant-related pathway.” The significance value was calculated by NES \times P value (if P ≤ 0.05, significance = NES \times 1, while significance = 0).

**Figure 4.**

Loss of DSB repair-related genes sensitizes cancer cell lines to the IFN γ treatment. **A**, Western blotting analysis for the efficiency of *PAXIP1* sgRNAs. For gene knockout experiments, three independent sgRNAs targeting *PAXIP1* were used, with one sgRNA targeting *AAVS1* as control. β -Tubulin is the loading control. **B**, Cell growth under 10 ng/mL IFN γ treatment. (Continued on the following page.)

signaling, T cell-mediated immune response, and inflammatory response, were activated after IFN γ treatment (Supplementary Fig. S5B; Supplementary Table S4). The transcriptomic activation of IFN γ -mediated signaling was similar in the cells regardless of IFN γ sensitivity (Fig. 6A; Supplementary Table S4), suggesting that in our data, IFN γ resistance is not due to the failure of IFN γ to activate these pathways. Our analysis of an independent transcriptomic data set (GSE85898; ref. 15) corroborated that IFN γ -mediated signaling was similarly activated in both IFN γ -sensitive ($n = 3$) and IFN γ -resistant cells ($n = 3$) after IFN γ treatment (16 hours; Supplementary Fig. S5C and S5D; Supplementary Table S4).

To further exclude the possibility that IFN γ resistance in our data were due to the blockage of IFN γ signaling transduction, we analyzed ISGs to evaluate whether IFN γ stimulation upregulated these genes (41). We found that ISGs were upregulated upon IFN γ treatment not only in the IFN γ -sensitive cell lines but also in the IFN γ -resistant cell lines (Fig. 6B), data that were supported by analysis of an independent data set (GSE85898; ref. 15; Supplementary Fig. S5E). Moreover, in a published data set (GSE154996) obtained from human melanoma cell lines exposed to IFN γ *in vitro* (42), we found that the upregulation of the ISGs after IFN γ treatment was blocked in JAK1/2-defective melanoma cells ($n = 8$) compared with wild-type cells ($n = 45$; Supplementary Fig. S5F). Altogether, these results demonstrated that resistance to IFN γ can still occur, even though ISGs and IFN γ signaling pathways are activated.

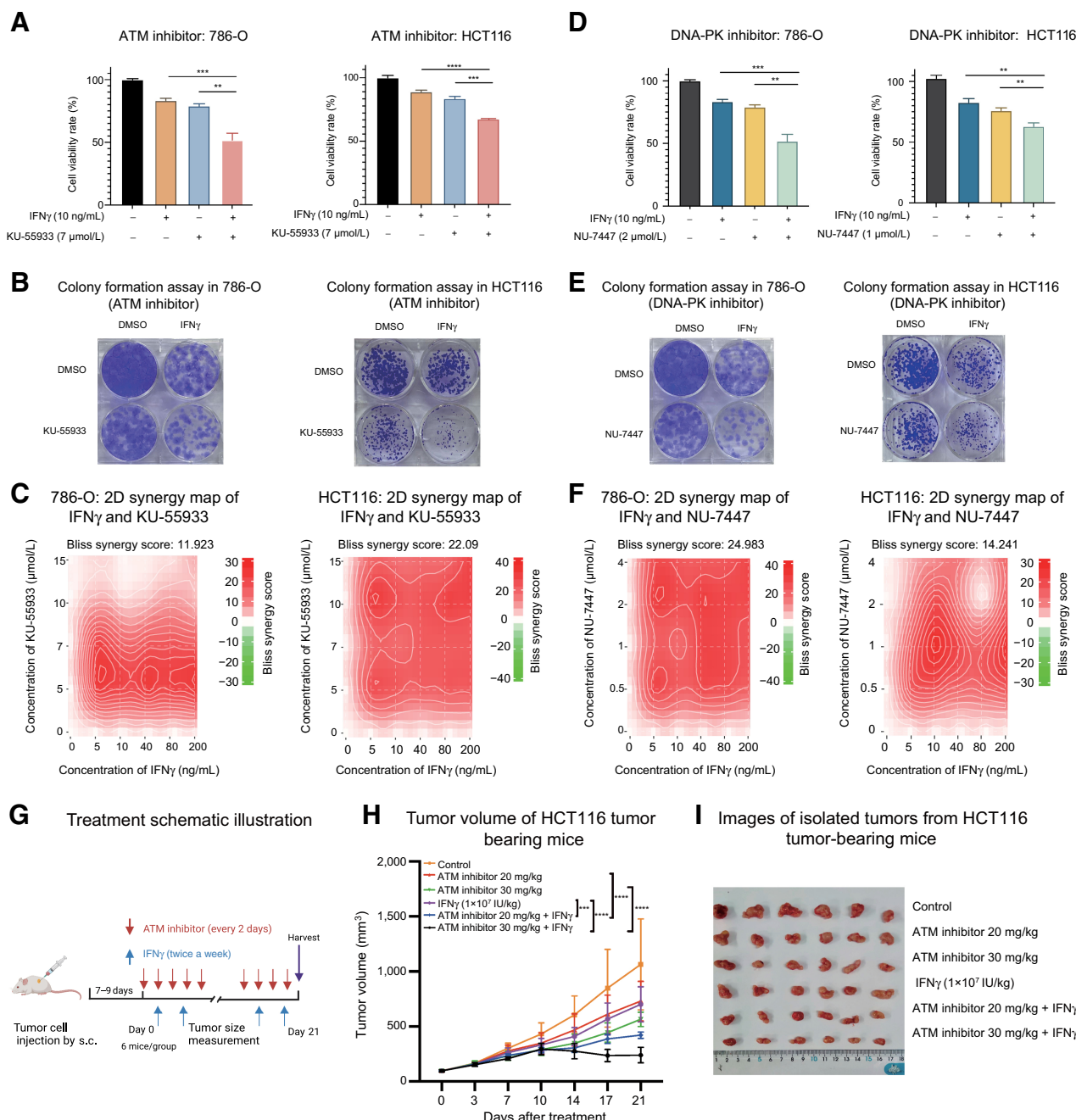
IFN γ influences cell viability by suppressing SSBr genes

The observation that ISGs were upregulated in both IFN γ -sensitive and IFN γ -resistant cell lines suggests that alternative mechanisms might drive IFN γ resistance. Because we found DSB repair genes to be highly expressed in IFN γ -resistant cell lines and essential for IFN γ resistance, we investigated whether IFN γ treatment could affect the expression of DSB repair genes. We performed pathway enrichment analysis for the downregulated genes after IFN γ treatment and focused on the DSB repair pathways, including recombinational repair, regulation of DSB repair via HR, and DSB repair. However, we did not observe significant downregulation of these pathways in either IFN γ -sensitive or IFN γ -resistant cell lines (Fig. 6C). Cooperation between DSB repair and SSBr is known to help cells preserve genome stability. These two repair pathways have a well-known synthetic lethality relationship, where loss of function of both can drive cancer cell apoptosis (43, 44). Considering that DSB repair genes were not significantly downregulated but had increased essentiality in IFN γ -resistant cell lines, we hypothesized that the increased essentiality of DSB repair genes in cancer cells might be due to inhibition of the SSBr genes upon IFN γ treatment.

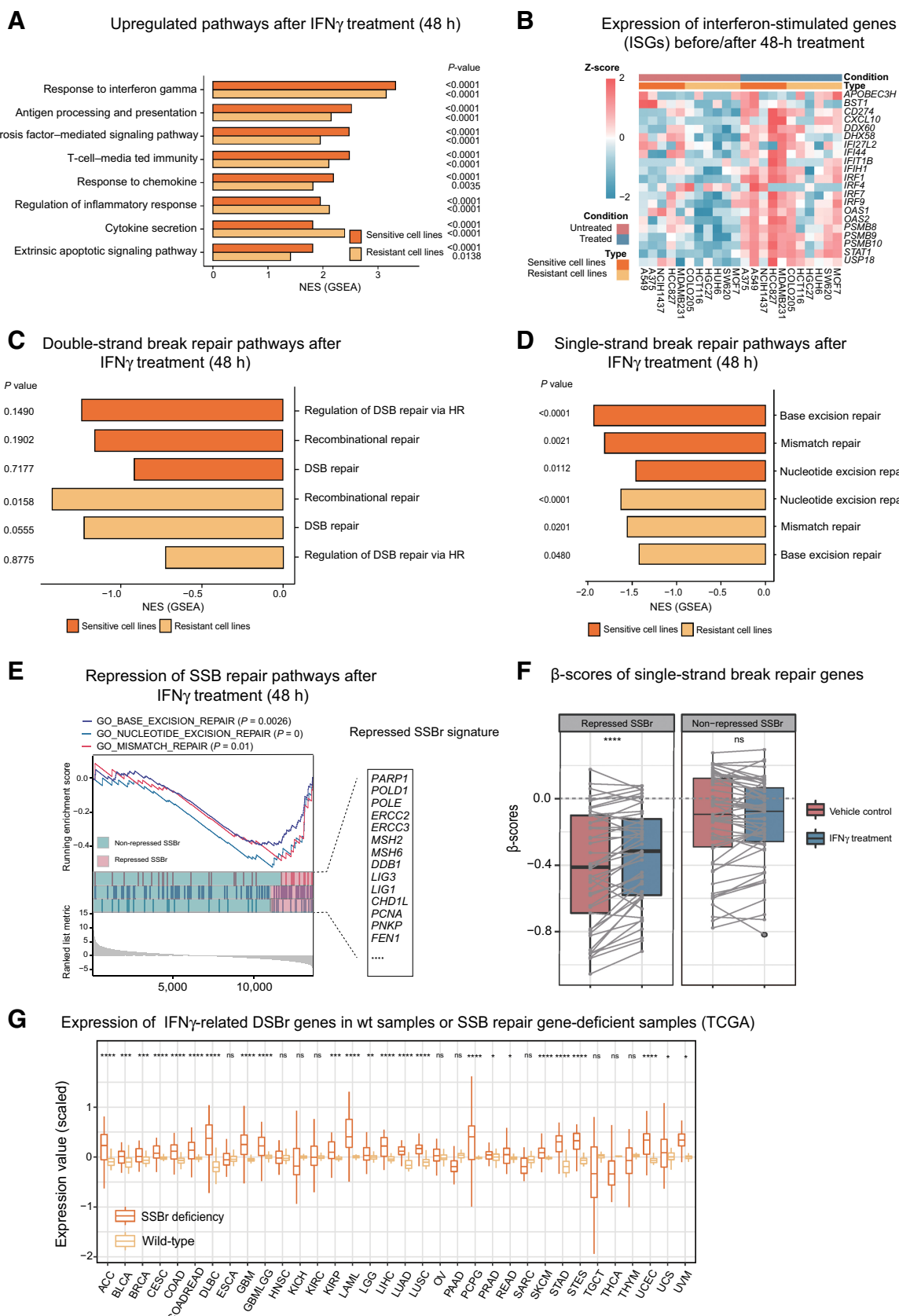
To address this issue, we examined the transcriptomic changes of SSBr genes upon IFN γ treatment. Genes related to SSBr pathways, such as mismatch-repair pathway (*MSH2* and *MSH6*), base excision repair pathway (*POLD1*, *PNKP*, and *FEN1*), and nucleotide excision repair pathway (*XPA*, *DDB1*, and *ERCC2/3*; ref. 45), were significantly downregulated after IFN γ treatment regardless of cell sensitivity to IFN γ (Fig. 6D and E). We used downregulated SSBr genes after IFN γ treatment to define a repressed SSBr gene signature (Fig. 6E; Supplementary Fig. S6A; Supplementary Table S5). To evaluate the universality of the repressed SSBr pathway upon IFN γ treatment, we performed similar analyses using the two public transcriptomic data sets where cancer cells were treated with IFN γ (GSE85898 and GSE154996; refs. 15, 42). We found that the repressed SSBr signature was significantly downregulated upon IFN γ treatment, suggesting a general effect of IFN γ on suppressing SSBr (Supplementary Fig. S6B and S6C). Moreover, we did not observe downregulation of repressed SSBr signature upon IFN γ treatment when the IFN γ cascade was blocked through the loss of *JAK1/2* (GSE154996; Supplementary Fig. S6D). Because many of these SSBr genes are reported to be involved in cell proliferation and cell cycle, we examined the effect of the repressed SSBr signature on cell viability in our CRISPR screens. Under vehicle control, genes in the repressed SSBr signature were negatively selected, indicating that these SSBr genes are important for cell viability (Fig. 6F; Supplementary Fig. S6E and S6F, pink box). However, under IFN γ treatment, which downregulates these repressed SSBr genes, the KO of these genes became less essential (Fig. 6F; Supplementary Fig. S6E and S6F, blue box). Collectively, these observations suggested that IFN γ treatment influences cell viability by inhibiting SSBr genes.

To evaluate whether cells with a deficiency of SSBr genes rely more on the intrinsic high expression of DSB repair genes for survival, we defined three different sets of DSB repair genes from our transcriptomic data under untreated conditions: (i) upregulated DSB repair genes in IFN γ -resistant cell lines (termed IFN γ -related DSBr); (ii) the nondifferentially expressed DSB repair genes (termed nonIFN γ -related DSBr), and (iii) all the DSB repair genes (all DSBr; Supplementary Table S5). Using CCLE data sets, we found that cells with truncating mutations (frameshift indels, nonsense, and splice-site mutations) or cells with copy-number deep deletions located in SSBr genes were associated with higher expression of DSB repair genes, especially the IFN γ -related DSBr genes (Supplementary Fig. S6G and S6H). We also made similar observations in the TCGA data set. In 70% (24 in 34) of the cancer types, tumors with SSBr genes deficiency had higher expression of IFN γ -related DSBr genes compared with tumors with wild-type SSBr genes (Fig. 6G; Supplementary Table S6). Thus, the high activity of DSB repair genes was associated with enhanced viability of the cancer cells with SSBr deficiency, suggesting a

(Continued.) 786-O cancer cell harboring three different sgRNAs targeting *PAXIP1* and one sgAAVS1 as control. The data are represented as mean \pm SD ($n = 3$; ns > 0.05; *, $P \leq 0.05$; **, $P \leq 0.01$; ***, $P \leq 0.001$; ****, $P \leq 0.0001$) by two-way ANOVA. C, Colony formation assay of *PAXIP1* depletion under IFN γ treatment in 786-O. Shown are the results from one representative experiment of two replicates. D, Western blotting analysis for the overexpression of *PAXIP1* in A549 (left); cell growth under 10 ng/mL IFN γ treatment (middle). A549 cancer cells harboring *PAXIP1* overexpression (lenti-*PAXIP1*) or one control (lenti-HA) were treated with IFN γ (10 ng/mL). The data are represented as mean \pm SD ($n = 6$; ns > 0.05; *, $P \leq 0.05$; **, $P \leq 0.01$; ***, $P \leq 0.001$; ****, $P \leq 0.0001$) by two-way ANOVA. Colony formation assay of *PAXIP1*-overexpressed A549 or control group (lenti-HA) treated with IFN γ (10 ng/mL, right). Shown are the results from one representative experiment of two replicates. E, Heat map showing the highly expressed gene sets (Z-score) in IFN γ -sensitive/resistant cells under untreated conditions. Differential expressed DSB repair genes (75 genes; denoted as IFN γ -related DSBr) are labeled in the box. F and G, Loss of function of (F) *RAD50* and (G) *RAD51* sensitizes 786-O to IFN γ treatment. Western blotting analysis for efficiency of *RAD50* and *RAD51* sgRNAs. For the gene knockout experiment, two independent sgRNAs were used, with one sgAAVS1 as control. β -Tubulin is the loading control. Cell growth under 10 ng/mL IFN γ treatment. 786-O cancer cell harboring the different sgRNAs targeting *RAD50* and *RAD51* sensitizes 786-O to IFN γ treatment. The data are represented as mean \pm SD ($n = 3$; ns > 0.05; *, $P \leq 0.05$; **, $P \leq 0.01$; ***, $P \leq 0.001$; ****, $P \leq 0.0001$) by two-way ANOVA. Colony formation assay of *RAD50* and *RAD51* depletion under IFN γ treatment in 786-O. Shown are the results from one representative experiment of two replicates.

**Figure 5.**

Inhibition of the DSB repair pathway overcomes resistance to IFN γ *in vitro* and *in vivo*. **A**, Bar plot showing the cell viability of 786-O and HCT116 treated with KU-55933 (ATM inhibitor) or/and IFN γ ; mean \pm SD for $n = 3$; two-tailed Student *t* test: * $P \leq 0.05$; ** $P \leq 0.01$; *** $P \leq 0.001$; **** $P \leq 0.0001$. **B**, Colony formation assay for 786-O and HCT116 under treatment of ATM inhibitor (KU-55933) and IFN γ . **C**, The 2D drug synergy map between ATM inhibitor (KU-55933) and IFN γ in 786-O and HCT116. The synergy score was calculated based on the Bliss independence model. The synergy scores are larger than 10, indicating that the two drugs are likely synergistic. **D**, Bar plot showing the cell viability of 786-O and HCT116 treated with DNA-PK inhibitor (NU-7447) or/and IFN γ ; mean \pm SD for $n = 3$; two-tailed Student *t* test: ns > 0.05; * $P \leq 0.05$; ** $P \leq 0.01$; *** $P \leq 0.001$; **** $P \leq 0.0001$. **E**, Colony formation assay for 786-O and HCT116 under treatment of DNA-PK inhibitor (NU-7447) and IFN γ . **F**, The 2D drug synergy map between DNA-PK inhibitor (NU-7447) and IFN γ in 786-O and HCT116. The synergy score was calculated based on the Bliss independence model. **G**, Treatment schematic illustration of tumor-bearing mice in which HCT116 colon cancer cells were subcutaneously injected into the 6- to 8-week-old female BALB/c nude mice. After subcutaneous injection of tumor cells for 7–9 days (the volume of the tumor was approximately 100 mm 3), mice were divided into six groups ($n = 6$ mice per group): untreated, ATM inhibitor (20 or 30 mg/kg, intraperitoneal injection, every 2 days for 3 weeks), IFN γ treatment (1×10^7 IU/kg, intratumoral injection, twice a week for 3 weeks), and ATM inhibitor + IFN γ (same dose and routes of administration as monotherapy groups). **H**, Growth curves from HCT116 tumor-bearing mice. Six mice per group. Data are shown as the mean \pm SEM; ns > 0.05; * $P \leq 0.05$; ** $P \leq 0.01$; *** $P \leq 0.001$; **** $P \leq 0.0001$ by two-way ANOVA. **I**, Images of isolated tumors from HCT116 tumor-bearing mice for each treatment group at the study endpoint; the ruler scale is mm.



collaboration between the DSB repair pathway and the SSBr pathway in cell survival. Altogether, our data revealed that IFN γ treatment suppresses the expression of SSBr genes, and cells with intrinsic high expression of DSB repair genes can sustain cell growth, thus conferring IFN γ resistance.

Increased DSB repair genes attenuate the beneficial effect of IFN γ on survival

We extended our findings to clinical data by investigating whether DSB repair genes influence the effect of IFN γ on clinical outcomes using data from TCGA cohorts (Fig. 7A). Among all the cancer types, higher *IFNG* expression was positively associated with better survival in melanoma (TCGA-SKCM), breast cancer (TCGA-BRCA), sarcoma (TCGA-SARC), and bladder cancer (TCGA-BLCA; Supplementary Table S7). Interestingly, in melanoma and breast cancer patients, higher *IFNG* expression was associated with better overall survival only when the IFN γ -related DSBr genes were lowly expressed (Fig. 7B; Supplementary Fig. S7A–S7C). Considering that other factors such as tumor stage/purity, patients' age, and CD8 $^+$ T-cell infiltration can dramatically affect survival (46), we revised a computational model TIDE to exclude the influence of these confounders on patients' survival (47). For each gene, we defined an IFN γ dysfunction score (IDS) based on the interaction effect of this gene and *IFNG* on patients' survival, with adjustment for clinical confounders (Supplementary Fig. S7D). A larger IDS indicated that higher expression of a gene would decrease the beneficial effect of *IFNG* on overall survival. Consistently, we observed significantly higher IDSs of the IFN γ -related DSBr in SKCM, BRCA, and SARC (Fig. 7C; Supplementary Fig. S7E and S7F). In BLCA, we did not observe higher IDSs (Supplementary Fig. S7G), which might be due to frequent alterations of DSB repair genes in bladder tumors (48). We also tested whether the mutation of DSB repair genes could alter the beneficial effect of *IFNG* on overall survival. Although there was a slight trend that IFN γ -related DSBr genes had a lower interaction coefficient compared with non-IFN γ -related DSBr, these genes did not reach a significant *P* value, which may be due to the extremely low frequency of DSB repair genes' alterations (Supplementary Fig. S7H). Mutations of IFN γ -related DSBr genes such as *PAXIPI*, *RAD51*, and *TP53BP1* were the top enriched genes with negative interaction coefficients suggesting potential roles of these genes in IFN γ resistance (Supplementary Fig. S7I). Altogether, these results indicated that DSB repair genes could attenuate the beneficial effect of IFN γ on patients' survival.

The benefit of ICB therapy has been reported to depend on IFN γ production (49). We investigated whether the DSB repair genes could also attenuate the effect of IFN γ on ICB response. Among three ICB clinical cohorts with a sample size larger than 40 (27–29), two cohorts showed significantly improved overall survival in patients with higher

IFNG expression (Supplementary Table S7). In line with our TCGA results, we found that higher *IFNG* expression was associated with better overall survival in the samples only when IFN γ -related DSBr genes were lowly expressed (Fig. 7D; Supplementary Fig. S8A). In addition, we observed significantly higher IDSs of IFN γ -related DSBr genes in these two ICB cohorts, indicating that IFN γ -related DSBr genes might attenuate the beneficial effect of *IFNG* on survival and affect patients' response to ICB (Fig. 7E; Supplementary Fig. S8B). Collectively, our study provides comprehensive data resources and reveals the upregulation of DSB repair genes as a mechanism underlying IFN γ resistance in cancer cells (Supplementary Fig. S8C). It also suggested that DSB repair gene activation-mediated tumor immune evasion through IFN γ resistance could be a predictive biomarker of ICB response.

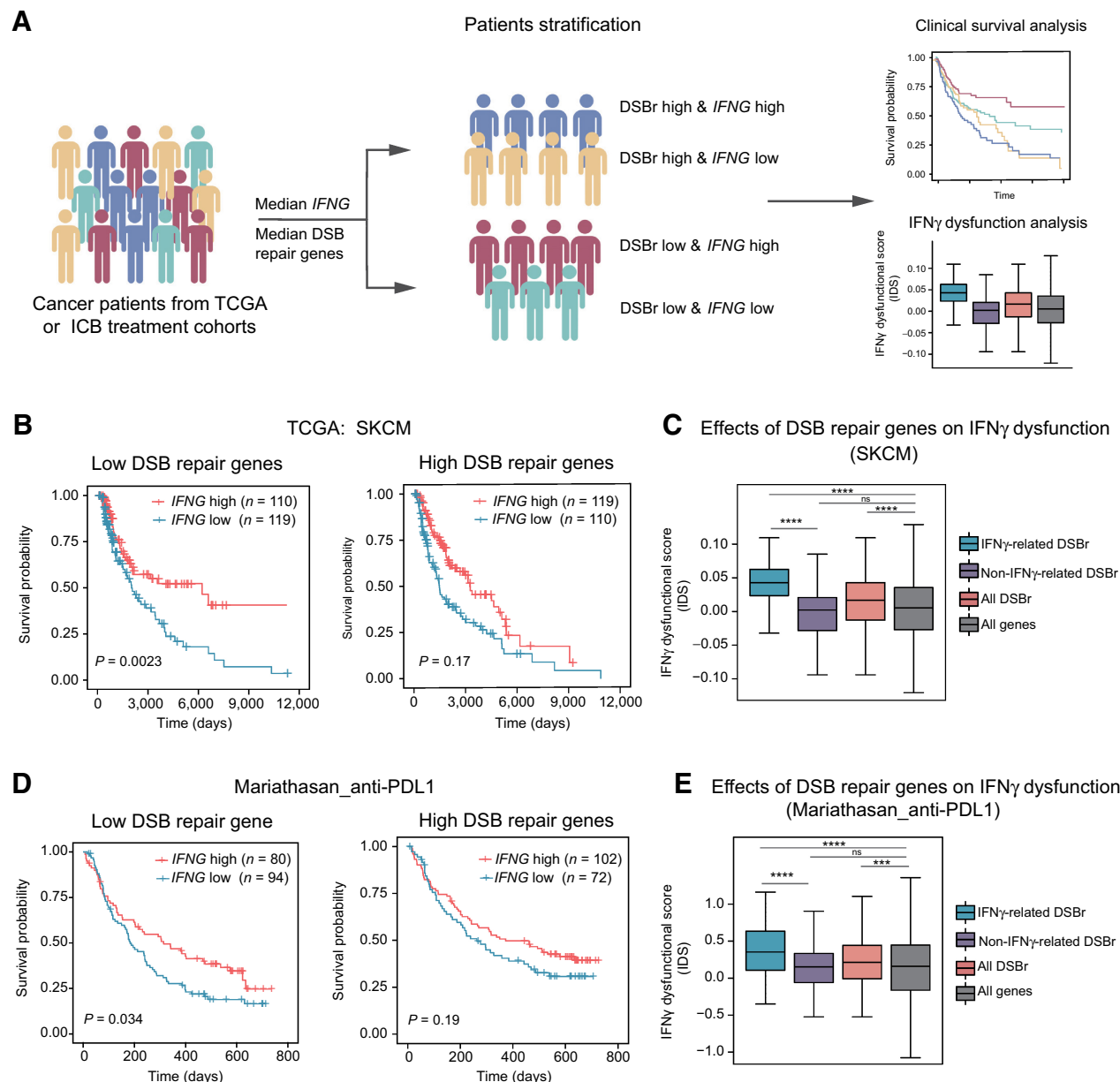
Discussion

Although extensive efforts have been made to understand IFN γ resistance, most of these studies focused on the defects in IFN γ signaling pathways. However, deficiency of the IFN γ signaling pathway was reported in fewer than 1% of patients (21). Given the lack of a comprehensive understanding of IFN γ resistance, it is critical to identify novel resistance mechanisms. In our study, we performed IFN γ -sensitivity screens in more than 40 cancer cell lines to evaluate the cell sensitivity. By leveraging the CCLE and our custom transcriptomic data set of these cancer cells, we uncovered that DSB repair genes were highly expressed in IFN γ -resistant cell lines. Functional CRISPR screens supported the associations between DSB repair genes and IFN γ resistance, and combined inhibition of DSB repair and IFN γ treatment overcame IFN γ resistance *in vitro* and *in vivo*. In addition, the results of the CRISPR screens suggested a potential synthetic lethality between DSB and SSBr genes, which were confirmed by analysis of publicly available CCLE and TCGA cohorts. Finally, we demonstrated that higher activity of DSB repair genes might be a general mechanism to evade IFN γ -mediated tumor cell killing and affect response to ICB in clinical cohorts. In summary, our study indicates potential mechanisms of IFN γ resistance and provides a potential strategy to enhance IFN γ treatment via a combination of DSB repair inhibition with IFN γ treatment.

Functional genomic screening using CRISPR-Cas9 has shown promise as a robust and unbiased approach to discovering novel cancer targets (50). In previous studies, *in vivo* CRISPR screens in murine melanoma models have revealed that loss of *PTPN2* and *ADARI* can enhance tumor sensitivity to immunotherapy through the IFN γ -mediated signaling pathway (20, 51). Our *in vitro* CRISPR screens also showed that loss of function of *PTPN2* or *ADARI* could sensitize cancer cells to IFN γ treatment. In addition, the genes that are

Figure 6.

IFN γ treatment analysis in IFN γ -sensitive/resistant cell lines. **A**, Pathway enrichment of upregulated genes in IFN γ -sensitive cell lines or IFN γ -resistant cell lines, respectively, after 48-hour IFN γ treatment. **B**, Heat map showing the expression (Z-score) of ISGs in both IFN γ -sensitive/resistant cell lines before/after IFN γ treatment (48 hours). **C** and **D**, Pathway enrichment of (**C**) DSB repair pathways or (**D**) SSBr pathways after 48-hour IFN γ treatment in both IFN γ -sensitive cell lines and IFN γ -resistant cell lines, respectively. **E**, GSEA for SSBr pathways after IFN γ treatment (across all the cells). The corresponding gene set IDs are NUCLEOTIDE_EXCISION_REPAIR (NES = -1.78, *P* = 0), BASE_EXCISION_REPAIR (NES = -1.92, *P* = 0.0026), and MISMATCH_REPAIR (NES = -1.69, *P* = 0.01). Downregulated SSBr genes after IFN γ treatment in these pathways were used to generate a gene signature called repressed SSBr (repressed SSBr, pink bar). Other SSBr genes are nonrepressed SSBr signatures (nonrepressed SSBr, green bar). Genes in repressed SSBr signature are labeled in the box. **F**, Boxplot showing the β -scores of repressed SSBr or nonrepressed SSBr under different conditions in CRISPR screens. A two-sided paired Student *t* test was used to compute the *P* value (ns > 0.05; *, *P* ≤ 0.05; **, *P* ≤ 0.01; ***, *P* ≤ 0.001; ****, *P* ≤ 0.0001). **G**, Expression of IFN γ -related DSBr genes in tumors with wild-type SSBr genes or tumors with SSBr genes deficiency in TCGA. In TCGA cancer types, there are 35 cancer types with copy-number deep deletions data (excluding KIPAN), and there are 34 cancer types with more than one sample with SSBr genes deficiency (excluding CHOL). A one-sided paired *t* test was used to compute the *P* value (ns > 0.05; *, *P* ≤ 0.05; **, *P* ≤ 0.01; ***, *P* ≤ 0.001; ****, *P* ≤ 0.0001).

**Figure 7.**

Increased DSB repair genes attenuate the beneficial effect of IFN γ on survival. **A**, Patient stratification. Patients from TCGA or ICB treatment cohorts were divided into four groups according to the median expression of *IFNG* and DSB repair genes. “DSBr High & *IFNG* High”: patients with above median expression of DSBr and *IFNG*. “DSBr High & *IFNG* Low”: patients with above median expression of DSBr but below median expression of *IFNG*. “DSBr Low & *IFNG* High”: patients with below median expression of DSBr but above median expression of *IFNG*. “DSBr Low & *IFNG* Low”: patients with both below median expression of *IFNG* and DSBr genes. Patients with different groups will be followed by survival analysis or IFN γ dysfunction analysis. **B**, The association between the *IFNG* level and overall survival for patients with different expressions of IFN γ -related DSBr genes in melanoma cohorts (SKCM) from TCGA. “*IFNG* High” or “*IFNG* Low” means the patients with above/below median *IFNG* expression value among all samples. “High DSB repair genes” or “Low DSB repair genes” refers to the samples with above/below median expression of DSB repair genes among all samples. Log-rank test was used to compute the P value in survival analysis. **C**, Boxplot showing the effects of DSB repair genes on IFN γ dysfunction in melanoma cohorts (SKCM-TCGA). The blue boxplot indicates IFN γ -related DSBr (IFN γ -related DSBr) genes (IFN γ -related DSBr genes defined in Fig. 4E; Supplementary Table S5); the purple box indicates the non-IFN γ -related DSBr (non-IFN γ -related DSBr) genes; the pink box indicates all DSBr (all DSBr) genes (GO:0006302). The gray box indicates all genes as background. A two-sided paired Student t test was used to compute the P value (ns > 0.05; *, P ≤ 0.05; **, P ≤ 0.01; ***, P ≤ 0.001; ****, P ≤ 0.0001). **D**, The association between the *IFNG* level and overall survival for patients with different expressions of IFN γ -related DSBr genes in urothelial cancer patients pretreated with anti-PD-L1. “*IFNG* high” or “*IFNG* low” means patients with above/below median *IFNG* expression value among all samples. “High DSB repair genes” or “Low DSB repair genes” means samples with above/below median DSB repair genes’ expression value among all samples. Log-rank test was used to compute the P value in survival analysis. **E**, Boxplot showing the effects of DSB repair genes on IFN γ dysfunction in patients with urothelial cancer pretreated with anti-PD-L1. The blue box indicates IFN γ -related DSBr; the purple box indicates the non-IFN γ -related DSBr; the pink box indicates all DSBr (GO:0006302). A two-sided paired Student t test was used to compute the P value (ns > 0.05; *, P ≤ 0.05; **, P ≤ 0.01; ***, P ≤ 0.001; ****, P ≤ 0.0001).

known to confer IFN γ resistance, such as *STAG2*, and *SH2B3*, were also identified in our CRISPR screens (52, 53). These results reflect the efficiency of our *in vitro* CRISPR screens and the reliability of the data resources. By integrating the transcriptomic profiles and CRISPR screen data sets, we optimized functional pathways related to IFN γ resistance. Using generalized linear models, we showed that activation of DSB repair pathways is a key factor related to IFN γ resistance independent of deactivation of the IFN γ -mediated signaling pathway. Taken together, our CRISPR screens combined with transcriptomic profiles serve as valuable resources to systematically identify the genes underlying IFN γ regulation, and the method for integrated analysis could also be used to identify other regulatory mechanisms such as drug resistance.

Despite the aforementioned merits, our study also has several limitations that deserve future exploration. First, in the cancer cell lines, the mutation status of DNA-repair genes should be taken into consideration. We evaluated the mutations of DSB repair genes and found frameshift deletion or insertions in both IFN γ -resistant and IFN γ -sensitive cell lines. This suggests that loss/gain of functions of DNA-repair genes are common in cancer cell lines. Additionally, in our study, we observed that alterations of IFN γ -related DSBr genes have lower interaction coefficients with *IFNG*, indicating the potential benefits of alterations of these genes on the effect of IFN γ on patient survival. Second, the KO experiments showed that *PAXIP1* and other DSB repair genes confer IFN γ resistance. However, *PAXIP1* was reported to regulate not only DSB repair but also epigenetic modifications. Whether *PAXIP1*-related IFN γ resistance is fully dependent on DSB repair or partially through epigenetic mechanisms requires further investigation. Moreover, although we showed a synergistic effect between DSB repair inhibition and IFN γ *in vivo*, the synergistic effect was evaluated only in an immunodeficient mouse model. Further studies are needed to evaluate the synergistic effect in an immunocompetent mouse model. Third, in our study, we identified a cytotoxic effect of IFN γ treatment via repressing SSBr genes in tumor cells. The synthetic lethality between DSB and SSBr genes could potentially explain the resistance to IFN γ -mediated cell killing, but additional detailed experiments are needed to fully elucidate the mechanisms. It is interesting that our study also observed that increased expression of DNA methylation genes, similar to DSB repair genes, has an antagonistic function in *IFNG*-mediated survival. One potential explanation could be that DNA-stabilizing mechanisms, including DNA damage repair and DNA methylation, might play an important role in IFN γ resistance, and additional detailed experiments are needed to fully elucidate the mechanism (54). Recently, studies have reported that antitumor immunotherapy using CTLA-4 and PD-1 inhibitors can increase IFN γ production and lead to the elimination of cancer cells (4). Mounting evidence indicates that DNA damage response defects are

important in driving sensitivity and response to ICB (55). The potential role of DNA-repair pathways in IFN γ -mediated ICB resistance is less well investigated. Our study unravels a relationship between the DSB repair pathway and IFN γ resistance that may provide insight into overcoming IFN γ -mediated ICB resistance.

Authors' Disclosures

C. Wang reports grants from the National Natural Science Foundation of China and the Natural Science Foundation of Shanghai during the conduct of the study. No disclosures were reported by the other authors.

Authors' Contributions

T. Han: Conceptualization, resources, data curation, formal analysis, validation, investigation, methodology, writing—original draft, writing—review and editing. X. Wang: Conceptualization, resources, data curation, software, investigation, methodology, writing—review and editing. S. Shi: Resources, data curation, investigation. W. Zhang: Resources, data curation, software, investigation. J. Wang: Validation, investigation, writing—review and editing. Q. Wu: Resources, data curation, supervision, investigation, methodology. Z. Li: Resources, data curation, investigation. J. Fu: Resources, data curation, software, investigation. R. Zheng: Resources, data curation, software, investigation. J. Zhang: Methodology. Q. Tang: Resources, data curation, methodology. P. Zhang: Conceptualization, supervision, funding acquisition, writing—original draft. C. Wang: Conceptualization, resources, supervision, funding acquisition, methodology, writing—original draft, writing—review and editing.

Acknowledgments

The authors acknowledge X. Shirley Liu from Dana Farber Cancer Institute for the helpful discussion and suggestions. The authors acknowledge the authors from published studies for sharing their data on cancer cells/tumor profiling cohorts. This work was supported by the National Natural Science Foundation of China (32222026, 32170660, 31801059, 32000561, 81872290, 81972172, and 31801185), Shanghai Rising Star Program (21QA1408200), the Natural Science Foundation of Shanghai (21ZR1467600), Shanghai Science and Technology Committee (19XD1423200), and Shanghai Hospital Development Center (SHDC2020CR2020B). The authors thank the Bioinformatics Supercomputer Center of Tongji University for offering computing resources. The IFN γ -sensitivity screen in Fig. 1B and the schematic illustration of tumor-bearing mice in Fig. 5G were created with BioRender.com (<https://biorender.com/>).

The publication costs of this article were defrayed in part by the payment of publication fees. Therefore, and solely to indicate this fact, this article is hereby marked "advertisement" in accordance with 18 USC section 1734.

Note

Supplementary data for this article are available at Cancer Immunology Research Online (<http://cancerimmunolres.aacrjournals.org/>).

Received January 19, 2022; revised October 18, 2022; accepted January 6, 2023; published first January 11, 2023.

References

- Dunn GP, Koebel CM, Schreiber RD. Interferons, immunity and cancer immunoeediting. *Nat Rev Immunol* 2006;6:836–48.
- Windbichler GH, Hausmaninger H, Stummvoll W, Graf AH, Kainz C, Lahodny J, et al. Interferon-gamma in the first-line therapy of ovarian cancer: a randomized phase III trial. *Br J Cancer* 2000;82:1138–44.
- Kim JS, Park YM, Kim NY, Yun HK, Lee KJ, Kim BH, et al. Combination treatment with intrahepatic arterial infusion and intratumoral injection chemotherapy in patients with far-advanced hepatocellular carcinoma and arterioportal or arteriovenous shunts: preliminary results. *Korean J Hepatol* 2011;17:120–9.
- Garris CS, Arlauckas SP, Kohler RH, Trefny MP, Garren S, Piot C, et al. Successful anti-PD-1 cancer immunotherapy requires T cell-dendritic cell crosstalk involving the cytokines IFN- γ and IL-12. *Immunity* 2018;49: 1148–61.
- Fu T, He Q, Sharma P. The ICOS/ICOSL pathway is required for optimal antitumor responses mediated by anti-CTLA-4 therapy. *Cancer Res* 2011;71: 5445–54.
- Gocher AM, Workman CJ, Vignali DAA. Interferon- γ : teammate or opponent in the tumour microenvironment? *Nat Rev Immunol* 2021; 22:158–72.

7. Ikeda H, Old LJ, Schreiber RD. The roles of IFN gamma in protection against tumor development and cancer immunoediting. *Cytokine Growth Factor Rev* 2002;13:95–109.
8. Chin YE, Kitagawa M, Su W-CS, You Z-H, Iwamoto Y, Fu X-Y, et al. Cell growth arrest and induction of cyclin-dependent kinase inhibitor p21 WAF1/CIP1 mediated by STAT1. *Science* 1996;272:719–22.
9. Fulda S, Debatin KM. IFNgamma sensitizes for apoptosis by upregulating caspase-8 expression through the Stat1 pathway. *Oncogene* 2002;21: 2295–308.
10. Xu X, Fu XY, Plate J, Chong AS. IFN-gamma induces cell growth inhibition by Fas-mediated apoptosis: requirement of STAT1 protein for up-regulation of Fas and FasL expression. *Cancer Res* 1998;58:2832–7.
11. Yang M-Q, Du Q, Varley PR, Goswami J, Liang Z, Wang R, et al. Interferon regulatory factor 1 priming of tumour-derived exosomes enhances the anti-tumour immune response. *Br J Cancer* 2018;118:62–71.
12. Melero I, Rouzaut A, Motz GT, Coukos G. T-cell and NK-cell infiltration into solid tumors: a key limiting factor for efficacious cancer immunotherapy. *Cancer Discov* 2014;4:522–6.
13. Beatty G, Paterson Y. IFN-gamma-dependent inhibition of tumor angiogenesis by tumor-infiltrating CD4+ T cells requires tumor responsiveness to IFN-gamma. *J Immunol* 2001;166:2276–82.
14. Murtas D, Maric D, De Giorgi V, Reinboth J, Worschach A, Fetsch P, et al. IRF-1 responsiveness to IFN-γ predicts different cancer immune phenotypes. *Br J Cancer* 2013;109:76–82.
15. Gao J, Shi LZ, Zhao H, Chen J, Xiong L, He Q, et al. Loss of IFN-γ pathway genes in tumor cells as a mechanism of resistance to anti-CTLA-4 therapy. *Cell* 2016; 167:397–404.
16. Sucker A, Zhao F, Pieper N, Heeke C, Maltaner R, Stadtler N, et al. Acquired IFNγ resistance impairs anti-tumor immunity and gives rise to T-cell-resistant melanoma lesions. *Nat Commun* 2017;8:15440.
17. Dighe AS, Richards E, Old LJ, Schreiber RD. Enhanced in vivo growth and resistance to rejection of tumor cells expressing dominant negative IFN gamma receptors. *Immunity* 1994;1:447–56.
18. Lesinski GB, Zimmerer JM, Kreiner M, Trefry J, Bill MA, Young GS, et al. Modulation of SOCS protein expression influences the interferon responsiveness of human melanoma cells. *BMC Cancer* 2010;10:142.
19. Pike KA, Tremblay ML. TC-PTP and PTP1B: regulating JAK-STAT signaling, controlling lymphoid malignancies. *Cytokine* 2016;82:52–7.
20. Manguso RT, Pope HW, Zimmer MD, Brown FD, Yates KB, Miller BC, et al. In vivo CRISPR screening identifies Ptpn2 as a cancer immunotherapy target. *Nature* 2017;547:413–8.
21. Shin DS, Zaretsky JM, Escuin-Ordinas H, Garcia-Diaz A, Hu-Lieskovian S, Kalbasi A, et al. Primary resistance to PD-1 blockade mediated by JAK1/2 mutations. *Cancer Discov* 2017;7:188–201.
22. Yu G, Wang L-G, Han Y, He Q-Y. clusterProfiler: an R package for comparing biological themes among gene clusters. *OMICS* 2012;16:284–7.
23. Li Z, Wang B, Gu S, Jiang P, Sahu A, Chen C-H, et al. CRISPR screens identify essential cell growth mediators in BRAF inhibitor-resistant melanoma. *Genomics Proteomics Bioinformatics* 2020;18:26–40.
24. Sanjana NE, Shalem O, Zhang F. Improved vectors and genome-wide libraries for CRISPR screening. *Nat Methods* 2014;11:783–4.
25. Ianevski A, He L, Aittokallio T, Tang J, et al. SynergyFinder: a web application for analyzing drug combination dose-response matrix data. *Bioinformatics* 2017;33: 2413–5.
26. Wang X, Zhang Z, Qin W, Liu S, Liu C, Genchev GZ, et al. RePhine: an integrative method for identification of drug response-related transcriptional regulators. *Genomics Proteomics Bioinformatics* 2021;19:534–48.
27. Mariathasan S, Turley SJ, Nickles D, Castiglioni A, Yuen K, Wang Y, et al. TGFβ attenuates tumour response to PD-L1 blockade by contributing to exclusion of T cells. *Nature* 2018;554:544–8.
28. Gide TN, Quek C, Menzies AM, Tasker AT, Shang P, Holst J, et al. Distinct immune cell populations define response to anti-PD-1 monotherapy and anti-PD-1/anti-CTLA-4 combined therapy. *Cancer Cell* 2019;35:238–55.
29. Riaz N, Havel JJ, Makarov V, Desrichard A, Urba WJ, Sims JS, et al. Tumor and microenvironment evolution during immunotherapy with nivolumab. *Cell* 2017;171:934–49.
30. Maxwell JR, Yadav R, Rossi RJ, Ruby CE, Weinberg AD, Aguila HL, et al. IL-18 bridges innate and adaptive immunity through IFN-gamma and the CD134 pathway. *J Immunol* 2006;177:234–45.
31. Mburu YK, Wang J, Wood MA, Walker WH, Ferris RL. CCR7 mediates inflammation-associated tumor progression. *Immunol Res* 2006;36:61–72.
32. Li W, Köster J, Xu H, Chen C-H, Xiao T, Liu JS, et al. Quality control, modeling, and visualization of CRISPR screens with MAGeCK-VISPR. *Genome Biol* 2015; 16:281.
33. Wang T, Birsoy K, Hughes NW, Krupczak KM, Post Y, Wei JJ, et al. Identification and characterization of essential genes in the human genome. *Science* 2015;350: 1096–101.
34. Fritsch M, Günther SD, Schwarzer R, Albert M-C, Schorn F, Werthenbach JP, et al. Caspase-8 is the molecular switch for apoptosis, necroptosis and pyroptosis. *Nature* 2019;575:683–7.
35. Lawson KA, Sousa CM, Zhang X, Kim E, Akthar R, Caumanns JJ, et al. Functional genomic landscape of cancer-intrinsic evasion of killing by T cells. *Nature* 2020;586:120–6.
36. El-Hashemite N, Zhang H, Walker V, Hoffmeister KM, Kwiatkowski DJ. Perturbed IFN-gamma-Jak-signal transducers and activators of transcription signaling in tuberous sclerosis mouse models: synergistic effects of rapamycin-IFN-gamma treatment. *Cancer Res* 2004;64:3436–43.
37. Buckley NE, Hosey AM, Gorski JJ, Purcell JW, Mulligan JM, Harkin DP, et al. BRCA1 regulates IFN-gamma signaling through a mechanism involving the type I IFNs. *Mol Cancer Res* 2007;5:261–70.
38. Cardenas H, Jiang G, Thomas Pepin J, Parker JB, Condello S, Nephev KP, et al. Interferon-γ signaling is associated with BRCA1 loss-of-function mutations in high grade serous ovarian cancer. *NPJ Precis Oncol* 2019;3:32.
39. Herrero AB, Gutiérrez NC. Targeting ongoing DNA damage in multiple myeloma: effects of DNA damage response inhibitors on plasma cell survival. *Front Oncol* 2017;7:98.
40. Shrivastav M, De Haro LP, Nickoloff JA. Regulation of DNA double-strand break repair pathway choice. *Cell Res* 2008;18:134–47.
41. Liu H, Golji J, Brodeur LK, Chung FS, Chen JT, de Beaumont RS, et al. Tumor-derived IFN triggers chronic pathway agonism and sensitivity to ADAR loss. *Nat Med* 2019;25:95–102.
42. Grasso CS, Tsui J, Onyshchenko M, Abril-Rodriguez G, Ross-Macdonald P, Wind-Rotolo M, et al. Conserved interferon-γ signaling drives clinical response to immune checkpoint blockade therapy in melanoma. *Cancer Cell* 2020;38:500–15.
43. Bryant HE, Schultz N, Thomas HD, Parker KM, Flower D, Lopez E, et al. Specific killing of BRCA2-deficient tumours with inhibitors of poly(ADP-ribose) polymerase. *Nature* 2005;434:913–7.
44. Farmer H, McCabe N, Lord CJ, Tutt ANJ, Johnson DA, Richardson TB, et al. Targeting the DNA repair defect in BRCA mutant cells as a therapeutic strategy. *Nature* 2005;434:917–21.
45. Caldecott KW. DNA single-strand break repair and spinocerebellar ataxia. *Cell* 2003;112:7–10.
46. Sharma P, Hu-Lieskovian S, Wargo JA, Ribas A. Primary, adaptive, and acquired resistance to cancer immunotherapy. *Cell* 2017;168:707–23.
47. Jiang P, Gu S, Pan D, Fu J, Sahu A, Hu X, et al. Signatures of T cell dysfunction and exclusion predict cancer immunotherapy response. *Nat Med* 2018;24:1550–8.
48. Mouw KW. DNA repair pathway alterations in bladder cancer. *Cancers (Basel)* 2017;9:28.
49. Hoekstra ME, Bornes L, Dijkgraaf FE, Philips D, Pardieck IN, Toebe M, et al. Long-distance modulation of bystander tumor cells by CD8(+) T cell-secreted IFNγ. *Nat Cancer* 2020;1:291–301.
50. Pan D, Kobayashi A, Jiang P, Ferrari de Andrade L, Tay RE, Luoma AM, et al. A major chromatin regulator determines resistance of tumor cells to T cell-mediated killing. *Science* 2018;359:770–5.
51. Ishizuka JJ, Manguso RT, Cheruiyot CK, Bi K, Panda A, Iracheta-Vellve A, et al. Loss of ADAR1 in tumors overcomes resistance to immune checkpoint blockade. *Nature* 2019;565:43–48.
52. Ding S, Diep J, Feng N, Ren L, Li B, Ooi YS, et al. STAG2 deficiency induces interferon responses via cGAS-STING pathway and restricts virus infection. *Nat Commun* 2018;9:1485.
53. Ding L-W, Sun Q-Y, Edwards JJ, Fernández LT, Ran X-B, Zhou S-Q, et al. LNK suppresses interferon signaling in melanoma. *Nat Commun* 2019;10:2230.
54. Zhou D, Robertson D. Role of DNA methylation in genome stability. Cambridge, MA: Academic Press; 2016, pp. 409–24.
55. Zhao P, Li L, Jiang X, Li Q. Mismatch repair deficiency/microsatellite instability-high as a predictor for anti-PD-1/PD-L1 immunotherapy efficacy. *J Hematol Oncol* 2019;12:54.